

RESEARCH ARTICLE

FOXO1 regulates developmental lymphangiogenesis by upregulating CXCR4 in the mouse-tail dermis

Kenta Niimi^{1,2}, Misaki Kohara¹, Eriko Sedoh², Moe Fukumoto¹, Satoshi Shibata¹, Toshinori Sawano¹, Fumi Tashiro³, Satsuki Miyazaki³, Yoshiaki Kubota⁴, Jun-ichi Miyazaki³, Shinobu Inagaki^{1,*} and Tatsuo Furuyama^{2,*}

ABSTRACT

Lymphangiogenesis plays important roles in normal fetal development and postnatal growth. However, its molecular regulation remains unclear. Here, we have examined the function of forkhead box protein O1 (FOXO1) transcription factor, a known angiogenic factor, in developmental dermal lymphangiogenesis using endothelial cell-specific FOXO1-deficient mice. FOXO1-deficient mice showed disconnected and dilated lymphatic vessels accompanied with increased proliferation and decreased apoptosis in the lymphatic capillaries. Comprehensive DNA microarray analysis of the causes of *in vivo* phenotypes in FOXO1-deficient mice revealed that the gene encoding C-X-C chemokine receptor 4 (CXCR4) was the most drastically downregulated in FOXO1-deficient primary lymphatic endothelial cells (LECs). CXCR4 was expressed in developing dermal lymphatic capillaries in wild-type mice but not in FOXO1-deficient dermal lymphatic capillaries. Furthermore, FOXO1 suppression impaired migration toward the exogenous CXCR4 ligand, C-X-C chemokine ligand 12 (CXCL12), and coordinated proliferation in LECs. These results suggest that FOXO1 serves an essential role in normal developmental lymphangiogenesis by promoting LEC migration toward CXCL12 and by regulating their proliferative activity. This study provides valuable insights into the molecular mechanisms underlying developmental lymphangiogenesis.

KEY WORDS: FOXO, C-X-C chemokine receptor type 4 (CXCR-4), Lymphangiogenesis, C-X-C chemokine ligand 12 (CXCL-12), Tail dermis, Chemokine

INTRODUCTION

The lymphatic system participates in fluid homeostasis, immune cell trafficking and surveillance, and absorption of fatty acids from the small intestine. Congenital deficits in the lymphatic vasculature can result in embryonic lethality with severe edema and impaired immune reactions (Tammela and Alitalo, 2010). Lymphangiogenesis (the growth of new lymphatic vessels from pre-existing lymphatic vasculature) is associated with normal


embryonic development and diverse pathological conditions such as lymph node metastasis of malignant tumors, lymphedema distichiasis and inflammation (Kerjaschki, 2014; Tammela and Alitalo, 2010). However, despite its importance in various physiological and pathological conditions, the molecular mechanisms underlying lymphangiogenesis remain less understood than those involved in angiogenesis.

The first identified lymphatic-specific key regulators of developmental lymphangiogenesis were vascular endothelial growth factor (VEGF) C, VEGFD and their receptor VEGF receptor 3 (VEGFR3), which is expressed on the lymphatic endothelial cell (LEC) membrane (Achen et al., 1998; Enholm et al., 1998; Joukov et al., 1996; Yamada et al., 1997). Ligand binding to VEGFR3 activates downstream signaling molecules such as JNK, ERK and the PI3K/Akt pathway, resulting in cell proliferation, migration and LEC survival (Karkkainen and Petrova, 2000; Mäkinen et al., 2001). VEGFR3-deficient mice die at embryonic day (E) 9.5 because of cardiovascular failure before the emergence of lymphatic vessels (Dumont et al., 1998). Previous findings have also demonstrated that knockout (KO) of the *Vegfc* gene in mice impairs the formation of lymphatic vascular networks (Karkkainen et al., 2004). Moreover, it has previously been reported that fibroblast growth factor 2, angiopoietin 1, insulin-like growth factors 1 and 2, and platelet-derived growth factor BB contribute to lymphangiogenesis (Rinderknecht and Detmar, 2008). Recent data have highlighted several cases where established angiogenic signaling, such as Notch signaling (Krebs et al., 2000), ephrinB2/EphB4 signaling (Adams et al., 1999) and TGF β signaling (Ferrari et al., 2009), also play pivotal roles in developmental lymphangiogenesis (Niessen et al., 2011, 2014; Wang et al., 2010). Regarding the transcriptional regulation of lymphangiogenesis, the PROX1 transcription factor in lymphatic endothelium is an essential regulator of developmental lymphangiogenesis (Wigle and Oliver, 1999). Other transcription factors, such as GATA2, NFATC1, COUP-TFII and FOXC2, are also reported to be regulators of developmental lymphangiogenesis, lymphatic valve development or LEC specification (Kazenwadel et al., 2015; Kulkarni et al., 2009; Norrmén et al., 2009; Srinivasan et al., 2010).

Forkhead box (FOX) transcription factor O (FOXO) family proteins, such as FOXO1, FOXO3a, FOXO4 and FOXO6, are mammalian orthologs of the *Caenorhabditis elegans* DAF-16 protein, and control the expression of genes involved in apoptosis (i.e. *Bcl2l1* and *Fasl*), cell cycle progression (i.e. *Cdkn1a* and *Cdkn1b*), DNA damage repair (i.e. *Gadd45a*), cell metabolism (i.e. *G6pd*), oxidative stress resistance (i.e. *Cat* and *Sod2*) and other cellular functions (Accili and Arden, 2004; Eijkelenboom and Burgering, 2013; Huang and Tindall, 2007). The FOXO-family proteins are functionally rich downstream components of PI3K/Akt (Brunet et al., 1999). Akt phosphorylates FOXO proteins at

¹Group of Neurobiology, Division of Health Science, Osaka University Graduate School of Medicine, Yamadaoka 1-7, Suita, Osaka 565-0871, Japan. ²Kagawa Prefectural University of Health Sciences, Hara 281-1, Mure, Takamatsu, Kagawa 761-0123, Japan. ³Department of Stem Cell Regulation Research, Osaka University Graduate School of Medicine, Yamadaoka 2-2, Suita, Osaka 565-0871, Japan. ⁴Department of Anatomy, Keio University School of Medicine, 35-Shinanomachi, Shinjuku-ku, Tokyo 160-8582, Japan.

*Authors for correspondence (inagaki@sahs.med.osaka-u.ac.jp; furuyama@chs.pref.kagawa.jp)

 S.I., 0000-0002-2785-1214; T.F., 0000-0001-7349-103X

conserved sites and induces their nuclear export, which suppresses their transcriptional activities (Accili and Arden, 2004; Brunet et al., 1999; Huang and Tindall, 2007). We and other groups have previously demonstrated that the FOXO1 is essential for developmental angiogenesis through histological studies in FOXO1 KO mice (Fukumoto et al., 2018; Furuyama et al., 2004; Wilhelm et al., 2016). Furthermore, through an *in vitro* study, FOXO1-deficient LECs failed to migrate toward exogenous ATP, owing to decreased purinergic receptor P2Y1 expression (Niimi et al., 2017). In the present study, we aimed to investigate the physiological function of FOXO1 in lymphangiogenesis *in vivo*; to this end, we produced endothelial cell-specific FOXO1-deficient mice and observed developmental lymphangiogenesis, focusing on cellular functions such as proliferation, apoptosis and migration. Moreover, we examined FOXO1-dependent cell migration and proliferation activity *in vitro* using primary lymphatic endothelial cells.

RESULTS

FOXO1 was strongly expressed in the LEC nuclei during developmental lymphangiogenesis

We used the mouse-tail dermis as a model with which to study developmental lymphangiogenesis. Developmental lymphangiogenesis occurs in the tail dermis during early postnatal development [postnatal day (P) 0-8], where it forms characteristic hexagonal networks of lymphatic vasculature. The mouse tail is, therefore, a good model for investigating abnormal developmental lymphangiogenesis (Niessen et al., 2011, 2014; Xu et al., 2010). In order to observe normal lymphangiogenic processes in the tail dermis, we performed immunohistochemical staining at various postnatal stages (P1-5) in wild-type mouse-tail dermis using a LYVE1-specific antibody, a marker of the lymphatic vasculature. Our results show that the quadrangular disconnected networks observed at P1 gradually developed into hexagonal connected networks at P5 (Fig. S1A). Data from a previous study showed that the lymphatic vasculature of the tail dermis forms characteristic multi-ring-shaped structures known as lymphatic ring complexes (LRCs), many of which are involved in developmental lymphangiogenesis (Xu et al., 2010). Our immunohistochemistry demonstrated that LRCs gradually become more robust during P1-5 (Fig. S1B), and that some of the filopodia-like structures extend toward other LRCs during P1-4 (Fig. S1B, arrows). The layer where these mesh-patterned lymphatic vessels exist is referred to as middle layer. Moreover, compared with the middle layer, LYVE1-positive ascending lymphatic vessels were observed in deeper layers (hereafter, referred to as the deep layer) (Fig. 1A). Very thin LYVE1-positive lymphatic vessels were observed in the layer above the middle layer – hereafter referred to as the superficial layer of the P3 and P5 tail dermis (Fig. 1A). However, superficial lymphatic vessels were not present in the P1 dermis (Fig. 1A). A schematic image detailing the development of the tail dermal lymphatic vessels is shown in Fig. 1B. It is considered that lymphatic vessels grow from the deep layer upwards towards the superficial layer. Next, we investigated the localization of FOXO1 within the vasculature of the wild-type developmental tail dermis. Immunohistochemistry experiments revealed that FOXO1 was strongly expressed in the LEC nuclei of each layer of P1, P3 and P5 dermis (Fig. 1C, Fig. S1C). In Pecam1⁺ LYVE1⁻ blood vessels, FOXO1 was strongly expressed in the blood endothelial nuclei of the superficial layer of each stage (Fig. S1C,E). However, we observed weaker nuclear FOXO1 expression in the P5 middle and deep blood vasculature of each stage compared with the lymphatic vasculature (Fig. 1C,D, Fig. S1C,D). This suggests that FOXO1 KO

might have a more significant influence on the formation of lymphatic capillaries when compared with blood vessels, at least in the early postnatal tail dermis.

Tie2 Cre-mediated Foxo1 KO impaired developmental lymphangiogenesis along with abnormal LEC proliferation and cell death in mouse-tail dermis

To study the influence of FOXO1 on developmental lymphangiogenesis in the tail dermis, we first used a tamoxifen-inducible Tie2 (tyrosine kinase with immunoglobulin-like and EGF-like domain 2) -positive endothelial cell-specific *Foxo1* conditional KO mice: *Tie2-CreER^{T2}-Foxo1^{fllox/fllox}*. A *Tie2-CreER^{T2}-Foxo1^{fllox/fllox}* mouse injected with tamoxifen is hereafter referred to as *Foxo1^{Tie2KO}*. *Tie2-CreER^{T2}-Foxo1^{fllox/+}* mice were used as littermate controls. Tie2 expression in developmental lymphatic vessels has previously been reported (Morisada et al., 2005). The schedule of tamoxifen injection is shown in Fig. S2A. Immunohistochemical analysis of tail dermis and western blot analysis of lung lysate from KO pups revealed that FOXO1 was successfully knocked out (Fig. S2B,C). The body weight of KO pups significantly decreased at P5 (Fig. S2D). All KO pups died by P11 (Fig. S2E), although we could not find any macroscopic findings, such as hemorrhage and edema. Anti-LYVE1 immunohistochemical staining showed that there was a remarkable reduction in the lymphatic vasculature in the middle layer of the dermis of KO mice compared with the control dermis at P5 (Fig. S2F). Further study revealed that tamoxifen-induced Cre-mediation results in reduced lymphatic vessel length and in fewer branch points per LRC in *Foxo1^{Tie2KO}* mice compared with those of control mice at P5 (Fig. S2G-J). Moreover, lymphatic vessels were dilated in *Foxo1^{Tie2KO}* mice compared with control mice at P5 (Fig. S2G,K). Next, cell proliferation was evaluated by intraperitoneal BrdU injection. The results show that the number of BrdU-positive LECs per length was higher in *Foxo1^{Tie2KO}* dermis compared with the control dermis (Fig. S2L,M). Subsequently, we evaluated apoptosis by immunostaining using antibody against cleaved caspase 3. Results show that the number of apoptotic LECs was lower in *Foxo1^{Tie2KO}* dermis compared with the control dermis (Fig. S2N,O). Furthermore, we studied the blood capillaries present in the dermis of *Foxo1^{Tie2KO}* mice using anti-Pecam1 and anti-LYVE1 immunohistochemical staining (Fig. S3). Unlike the remarkable phenotype in the lymphatic vasculature, we observed only a slight increase in the length of blood capillaries in the superficial layer of *Foxo1^{Tie2KO}* dermis (Fig. S3A-G).

VE cadherin (Cdh5) Cre-induced Foxo1 KO resulted in abnormal dermal lymphatic development

As both endothelial and hematopoietic cells express *Tie2*, *Foxo1* was deleted in the endothelium and also in hematopoietic cells in the *Foxo1^{Tie2KO}* mice. Consequently, inactivation of *Foxo1* in hematopoietic cells may play a role in lymphangiogenesis. To assess this hypothesis, we investigated dermal lymphatic development in *Cdh5-CreER^{T2}-Foxo1^{fllox/fllox}* mice with tamoxifen-induced endothelial *Foxo1* KO. Tamoxifen-treated *Cdh5-CreER^{T2}-Foxo1^{fllox/fllox}* mice are hereafter referred to as *Foxo1^{Cdh5KO}*. The littermates of *Cdh5-CreER^{T2}-Foxo1^{fllox/+}* mice were used as controls. The schedule of tamoxifen injection was the same as that explained for *Tie2* Cre-mediated KO (Fig. 2A). Successful *Cdh5* Cre-mediated *Foxo1* KO was confirmed by immunohistochemical analysis of tail dermis and western blot analysis of lung lysates (Fig. 2B,C). The body weight of P5 *Foxo1^{Cdh5KO}* pups was significantly reduced compared with that of

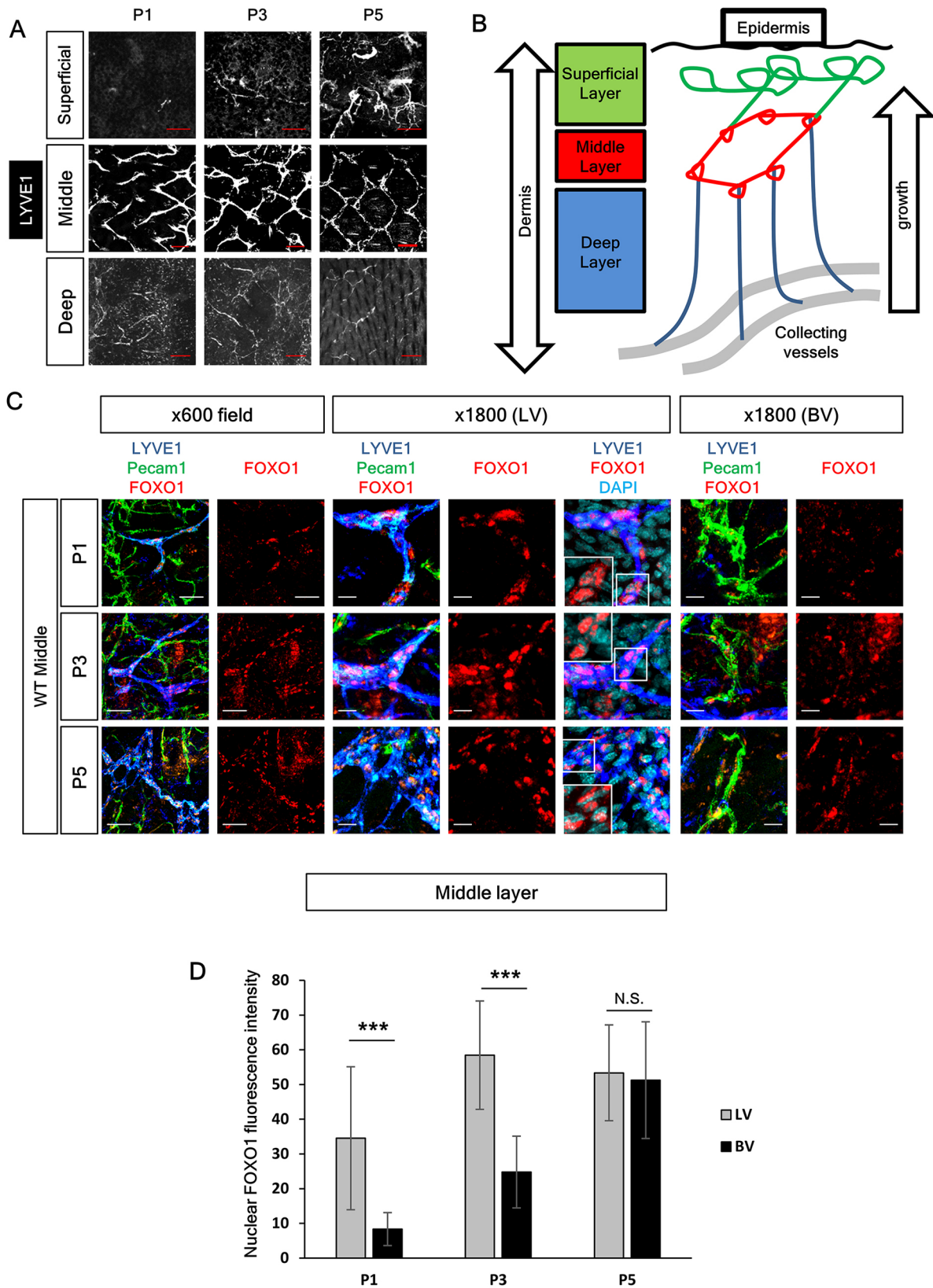


Fig. 1. Normal developmental lymphangiogenesis and FOXO1 localization in mouse-tail dermis. (A) LYVE1 immunostaining of tail dermis of wild-type mice at P1-P5 in each layer. (B) A schematic image of the hierarchical structure of tail dermal lymphatic vessels. (C) LYVE1 (blue), Pecam1 (green) and FOXO1 (red) immunostaining in the middle layer of wild-type tail dermis at P1, P3 and P5. White boxes outline the areas shown in more detail in the insets. (D) Quantification of nuclear FOXO1-positive fluorescence in LECs shown in C. Number of nuclei=50 (P1:LV), 55 (P3:LV), 66 (P5:LV), 40 (P1:BV), 41 (P3:BV) and 46 (P5:BV). Data are mean±s.d., *** $P < 0.001$, N.S., not significant. Scale bars: 100 μ m in A (middle and deep); 20 μ m in A (superficial) and C ($\times 600$); 5 μ m in C ($\times 1800$). LV, lymphatic vessels; BV, blood vessels.

control pups (Fig. 2D). Interestingly, unlike *Tie2* Cre-induced KO, ~70% of *Foxo1^{Cdh5KO}* pups survived until at least P21 (Fig. 2E). The dermal lymphatic phenotypes of P5 *Foxo1^{Cdh5KO}* pups were similar to *Foxo1^{Tie2KO}* pups, with reduced vessel length and branch points, increased vessel width, increased LEC proliferation, and decreased LEC apoptosis (Fig. 2F-O). We next performed anti-VEGFR3 immunostaining in P5 pups to assess the phenotype of collecting or pre-collecting lymphatic vessels. The length of collecting and pre-collecting lymphatic vessels was not altered in KO pups, while reduced branch points and increased width of collecting and pre-collecting lymphatic vessels were observed in KO pups compared with control pups (Fig. S4A-D). We also assessed mesenteric lymphatic vessels in P5 KO pups to determine whether the phenotypes are dermis specific or not. Anti-PROX1 immunostaining revealed that mesenteric lymphatic vessels were not affected in terms of branch points and width in KO pups (Fig. S5A-C). We also investigated the blood vessels of P5 *Foxo1^{Cdh5KO}* pups. Immunohistochemical studies showed that *Pecam1⁺* *LYVE1⁻* blood vessels were not different in terms of their length, branch points and diameter in middle layer (Fig. S6A,F-H). Interestingly, we found that blood vessel width in the superficial layer was dilated in *Foxo1^{Cdh5KO}* pups compared with control pups (Fig. S6A,K).

Prox1 Cre-induced Foxo1 KO resulted in abnormal dermal lymphatic development, as with Tie2 Cre-induced and Cdh5 Cre-induced KO

For more precise analysis of the *Foxo1* KO phenotype on lymphatic vasculature, we next used the *Prox1-CreER^{T2}-Foxo1^{lox/lox}* mouse, in which a *Foxo1* deficit was specifically induced in lymphatic vessels but not in blood vessels following tamoxifen treatment. Tamoxifen-treated *Prox1-CreER^{T2}-Foxo1^{lox/lox}* mice are hereafter referred to as *Foxo1^{Prox1KO}*. Littermates of *Prox1-CreER^{T2}-Foxo1^{lox/+}* mice were used as experimental controls. The schedule of tamoxifen injection was the same as that used in case of *Tie2* and *Cdh5* Cre-mediated KO (Fig. S7A). Immunohistochemical analysis of tail dermis and western blot analysis of lung lysates showed successful *Foxo1* KO in the lymphatic vasculature of *Foxo1^{Prox1KO}* pups (Fig. S7B,C). The fitness of *Foxo1^{Prox1KO}* pups was good at P5. The body weight of *Foxo1^{Prox1KO}* pups was not different from control pups (Fig. S7D). All *Foxo1^{Prox1KO}* mice survived until P21 (Fig. S7E). The dermal lymphatic abnormalities in P5 *Foxo1^{Prox1KO}* pups were similar to those observed in *Foxo1^{Tie2KO}* and *Foxo1^{Cdh5KO}* pups; these mice had reduced vessel length and branch points, dilated vessels, increased numbers of BrdU-positive LECs and decreased cleaved caspase 3-positive LECs (Fig. S7F-O).

Early postnatal Cdh5 Cre-induced Foxo1 KO resulted in long-term abnormalities in the lymphatic vasculature

The following analysis was performed with *Foxo1^{Cdh5KO}* mice because they allow for long-term analysis and have the most severe lymphatic vasculature phenotypes. It is possible that FOXO1-independent pathways correct the lymphatic abnormalities observed in *Foxo1*-deficient vasculature in the long term. To investigate this possibility in *Foxo1^{Cdh5KO}* mice, we treated mice with tamoxifen at P1, P2 and P3, and subsequently harvested tail dermis at P8 or P21 (Fig. 3A). Efficient *Foxo1* KO in the lymphatic vasculature was confirmed by dermal immunohistochemistry and western blot analysis of lung lysates (Fig. S8A-D). Similar to P5, we found that at P8 there was a reduction in middle lymphatic vessel length and branch points compared with control mice (Fig. 3B,D,E). We also observed dilated lymphatic vessels in the middle layer of

Foxo1^{Cdh5KO} mice (Fig. 3B,F), but total lymphatic vessel length was not altered in the superficial layer of *Foxo1^{Cdh5KO}* mice compared with control mice (Fig. 3B,C). At P21, dermal lymphatic capillaries were properly connected and they covered the whole tail dermis in both control and *Foxo1^{Cdh5KO}* mice (data not shown). Total lymphatic vessel length in the middle layer was not altered (Fig. 3G,I). However, at P21, we observed increased diameter and a reduction in the number of branch points per LRC in the middle layer of *Foxo1^{Cdh5KO}* mice compared with control mice as with P5 and P8 (Fig. 3G,J,K). Interestingly, unlike at P8, the total length of lymphatic capillaries in the superficial layer at P21 decreased in *Foxo1^{Cdh5KO}* mice compared with control mice (Fig. 3G,H).

Endothelial Foxo1 inactivation in the later period of dermal lymphatic development also altered lymphatic vessel formation

To investigate whether the time points for tamoxifen treatment affected lymphatic development in *Foxo1^{Cdh5KO}* mice, we injected mice with tamoxifen at P4 and P5 or P6 and P7, and subsequently sacrificed and harvested tail dermis at P8 (Fig. 4A). Successful *Foxo1* KO in lymphatic vasculature was confirmed by dermal immunohistochemistry and western blot using lung lysate (Fig. S8E-H). When we injected tamoxifen at P4 and P5, we found that the total lymphatic vessel length, number of branch points per LRC and lymphatic vessel diameter in the middle layer were not altered in *Foxo1^{Cdh5KO}* mice compared with control mice (Fig. 4B,D-F). However, the total vessel length of superficial lymphatic capillaries was decreased in *Foxo1^{Cdh5KO}* mice compared with that of control mice (Fig. 4B,C). When tamoxifen was injected at P6 and P7, total lymphatic vessel length in the middle layer was also not altered in *Foxo1^{Cdh5KO}* mice compared with control mice (Fig. 4G,I). However, the branch point count per LRC was reduced and the lymphatic vessel in the middle layer was slightly dilated in *Foxo1^{Cdh5KO}* mice compared with control mice (Fig. 4G,J,K). Interestingly, the total vessel length of superficial lymphatic capillaries was not altered in *Foxo1^{Cdh5KO}* mice compared with control mice (Fig. 4G,H). The results of long-term analysis and injection-point analysis are summarized in Fig. 4L.

Foxo1 KO decreased C-X-C chemokine receptor 4 (CXCR4) expression

To investigate the cause of lymphatic phenotypes in *Foxo1* KO dermis, we performed complementary DNA (cDNA) microarray analysis using cDNA samples from primary human dermal LECs (HDLECs) transfected with *FOXO1*-specific small interfering RNA (siRNA; siFOXO1) or a negative-control siRNA (siNC). *FOXO1* knockdown using siFOXO1 was successful (Fig. 5B). The cDNA microarray results are shown in Tables S1 and S2 as the log ratios of the target-gene expression levels in siFOXO1 versus siNC transfectants. Among these genes, expression of *CXCR4* was especially decreased in siFOXO1-transfected HDLECs when compared with that in siNC-transfected HDLECs (Table S1), as confirmed by quantitative RT-PCR (qRT-PCR; Fig. 5A). Furthermore, using western blotting and immunocytochemical analysis, we found that *CXCR4* levels were downregulated in *FOXO1* knock-down HDLECs (Fig. 5B,C). *CXCR4* and its ligand, C-X-C chemokine ligand 12 (CXCL12), form a signaling axis that is involved in normal development of the hematopoietic, cardiovascular, renal and nervous systems (Mithal et al., 2013; Nagasawa et al., 1996; Siervo et al., 2007; Takabatake et al., 2009). In fact, previous findings have revealed that the *CXCR4/CXCL12* axis contributes to physiological and pathological angiogenesis

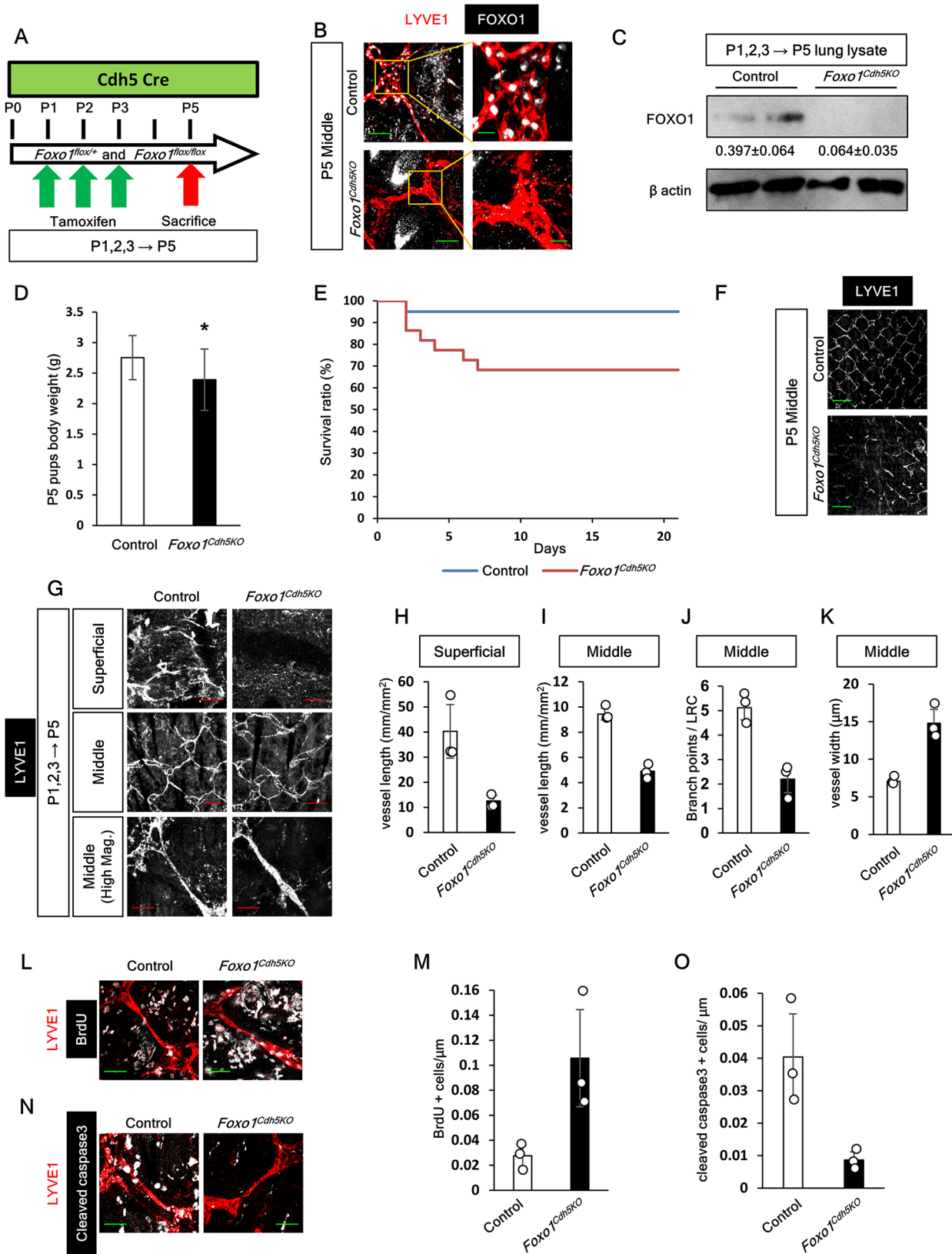


Fig. 2. See next page for legend.

through its chemotactic activity, both *in vitro* and *in vivo* (Mirshahi et al., 2000; Ping et al., 2011; Salcedo et al., 1999; Strasser et al., 2010). Based on these findings, we performed immunohistochemical

staining with CXCR4-specific antibodies using tail dermis from P1, P3 and P5 wild-type mice. We used an anti-CXCR4 antibody (clone UMB2) that specifically recognizes the non-phosphorylated CXCR4

Fig. 2. Abnormal developmental lymphangiogenesis in *Foxo1^{Cdh5KO}* mice tail dermis. (A) Schematic of tamoxifen injection for *Cdh5* promoter-dependent *Foxo1* deletion *in vivo*. (B) Immunostaining image of the FOXO1 (gray) and LYVE1 (red) in the tail dermis of control and *Foxo1^{Cdh5KO}* mice at P5. (C) Western blot analysis of FOXO1 protein using control and *Foxo1^{Cdh5KO}* mice lung lysate. Relative band intensities of FOXO1 to β -actin are shown as mean \pm s.d. (D) Body weight comparison between P5 control and *Foxo1^{Cdh5KO}* pups; $n=19$ for control mice and $n=16$ for *Foxo1^{Cdh5KO}* mice. Data are mean \pm s.d. * $P<0.05$. (E) Survival curve analysis of control and *Foxo1^{Cdh5KO}* mice; $n=20$ for control mice and $n=12$ for *Foxo1^{Cdh5KO}* mice. (F) Low-power magnification of LYVE1 immunostaining in the tail dermis from control and *Foxo1^{Cdh5KO}* mice at P5. (G) High-power magnification of LYVE1 immunostaining in the tail dermis from control and *Foxo1^{Cdh5KO}* mice at the P5 stage. (H,I) Total lymphatic vessel length based on the immunostaining image for LYVE1 was measured in superficial (H) and middle (I) layers. (J,K) Branch point number per LRC (J) and lymphatic vessel diameter in the middle layer (K) were also measured in P5 dermis. (L,M) Immunostaining images (L) showing LYVE1 (red) and BrdU (gray) in control and *Foxo1^{Cdh5KO}* mouse dermal lymphatic vasculatures. The pups were pre-injected with BrdU 1 h before they were sacrificed, and BrdU-positive cells per μ m vascular length were counted; $n=3$ for control mice and $n=3$ for *Foxo1^{Cdh5KO}* mice (M). (N,O) Immunostaining images of LYVE1 (red) and cleaved caspase 3 (gray) in control and *Foxo1^{Cdh5KO}* mouse dermal lymphatic vasculatures (N), and cleaved caspase-positive cell count per μ m vascular length (O); $n=3$ for control mice and $n=3$ for *Foxo1^{Cdh5KO}* mice. Scale bars: 200 μ m in F; 100 μ m in G (middle); 20 μ m in B (low magnification), G (superficial and middle, high magnification), L and N; 5 μ m in B (high magnification). All data are mean \pm s.d. * $P<0.05$.

protein. Therefore, absence of a signal using this antibody suggests that either CXCR4 is absent, or that all of the expressed CXCR4 is phosphorylated. For clarification, we performed pretreatment of whole tail dermis with lambda protein phosphatase (PP) before immunohistochemical staining. No signal post-PP treatment suggests that CXCR4 is absent. In the tail dermis of P1 wild-type mice, the CXCR4 protein was expressed on lymphatic capillaries in the middle and deep layers (Fig. 5D,H). However, in the P3 and P5 dermis of wild-type mice, the CXCR4 protein was only expressed in the lymphatic capillaries of the superficial layer, but not in the middle and deep layers (Fig. 5F-H). In the wild-type tail dermis that was not incubated with PP, the CXCR4 protein was not detected in lymphatic vessels at P1 (Fig. 5E), P3 or P5 stages (data not shown), indicating that all of the expressed CXCR4 protein in the lymphatic vessels of postnatal developing tail dermis is phosphorylated. To test CXCR4 reduction in *Foxo1*-KO dermis, we performed immunohistochemistry using anti-CXCR4 and anti-LYVE1 antibodies in the KO dermis and control dermis treated with PP at P3 and P5. However, it was difficult to show the CXCR4 reduction in P3 and P5 lymphatic capillaries because of the absence of superficial lymphatic vessels in the dermis of KO mice (Fig. S9A, B). As a result, we performed short-term KO analysis in the P1-2 dermal middle lymphatic vasculature that expressed CXCR4. Tamoxifen was injected 12 h after birth (P0.5) and tail dermis was harvested 36 h after birth (P1.5) (Fig. 6A). Efficient *Foxo1* KO was confirmed by dermal immunohistochemistry and western blot using lung lysate (Fig. 6B,C). Anti-CXCR4 and anti-LYVE1 immunohistochemical studies in the dermis of P1.5 mice treated with PP displayed a remarkable reduction in CXCR4 levels in the lymphatic vasculature of *Foxo1^{Cdh5KO}* dermis compared with control dermis (Fig. 6D,E). Furthermore, to identify the source of CXCL12, we performed immunohistochemistry with a CXCL12-specific antibody in control and *Foxo1^{Cdh5KO}* mice tail dermis. Results from these experiments revealed that CXCL12 was strongly expressed in the middle layer of the lymphatic vasculature but downregulated in superficial lymphatic capillaries (Fig. S10). The localization and signal intensity of CXCL12 were not altered by *Foxo1* KO (Fig. S10).

FOXO1 binds directly to the *Cxcr4* promoter and enhancer regions *in vitro*

In order to determine whether the FOXO1 protein drives CXCR4 expression, we performed luciferase reporter assays using luciferase reporter vectors containing variable-length segments of the mouse genomic *Cxcr4* region (497 bp, 224 bp or 75 bp upstream of the start codon). Among these, the 75 bp region of genomic *Cxcr4* corresponds to the 5'-UTR. The *Cxcr4* promoter region proximal to the transcription start site (TSS) is highly conserved between humans and mice (Fig. 7A). The strongest luciferase activity was observed following co-transfection with a reporter vector containing 224 bp or 497 bp of the *Cxcr4* genomic region, and a plasmid encoding a nuclear-localized constitutively active *Foxo1* mutant [FOXO1(CA)] (Fig. 7B). The 5'-UTR had no luciferase activity (Fig. 7B). The results suggest that the 149 bp region upstream of the TSS could be a potential target region of the FOXO1 protein. Furthermore, ChIP qPCR shows that anti-FOXO1 antibodies precipitated this region of the *CXCR4* promoter (Fig. 7C). Exon 2 of *CXCR4* (negative control) was not precipitated by anti-FOXO1 antibody (Fig. 7C). However, this region overlaps with a TATA box (Fig. 7A) and is not a typical FOXO1-binding element (FBE). Consequently, we next investigated the possibility that FOXO1 acts as a transcriptional factor in the upstream enhancer elements of the *CXCR4* gene. To identify the enhancer of this gene, we used the ENCODE database (the database of DNA functional elements; www.encodeproject.org/) and found H3K27ac binding (in HUVECs), FOXO1 binding (in B-lymphocyte) and a DNaseI hypersensitivity region \sim 120 kb upstream from the TSS (Fig. 7D). Within that region, we found a \sim 1.3 kb region with three FBEs (Fig. 7E), one of which is fully conserved between humans and mice (Fig. 7E). We performed anti-FOXO1 ChIP qPCR to amplify three different regions (regions 1-3) each containing one FBE (Fig. 7E). Region 3 contains the fully conserved FBE (Fig. 7E). The results show that region 3 was precipitated most abundantly by FOXO1 (Fig. 7F). This indicates that FOXO1 binds directly to the putative enhancer of the *CXCR4* gene in LECs.

Foxo1 knockdown affected CXCL12-dependent LEC migration *in vitro*

CXCL12 is reported to chemoattract CXCR4-expressing cells, and to mediate lymphocyte trafficking and immune functions (Bleul et al., 1996, 1997); however, its effects on LECs are still poorly understood. Therefore, we analyzed HDLEC migration towards CXCL12 gradients in collagen-coated, transwell membranes by counting Giemsa-stained migratory cells. HDLEC migration increased when the lower chamber contained 0.1-100 ng ml⁻¹ CXCL12; however, chemoattraction towards 1000 ng ml⁻¹ CXCL12 was marginal (Fig. 8A,B). Moreover, migration was inhibited by pre-incubation with 5 μ M of the CXCR4 antagonist AMD3100 (Fig. 8A,B). These results indicate that HDLECs migrate towards extracellular CXCL12 via CXCR4. As mentioned above, *FOXO1* knockdown led to downregulation of CXCR4 expression in HDLECs. It is therefore possible that *FOXO1* knockdown affected HDLEC migration towards CXCL12. To investigate this possibility, we examined the migration of siNC or siFOXO1 transfected HDLECs, transduced with adeno-associated viral EGFP vector (AAV-EGFP) or AAV-CXCR4, in collagen-coated transwell membranes containing 100 ng ml⁻¹ CXCL12. We found that AAV-CXCR4 could rescue the *Cxcr4* mRNA downregulation in siFOXO1 transfectants (Fig. 8C). The migration assay showed that HDLEC migration of siFOXO1

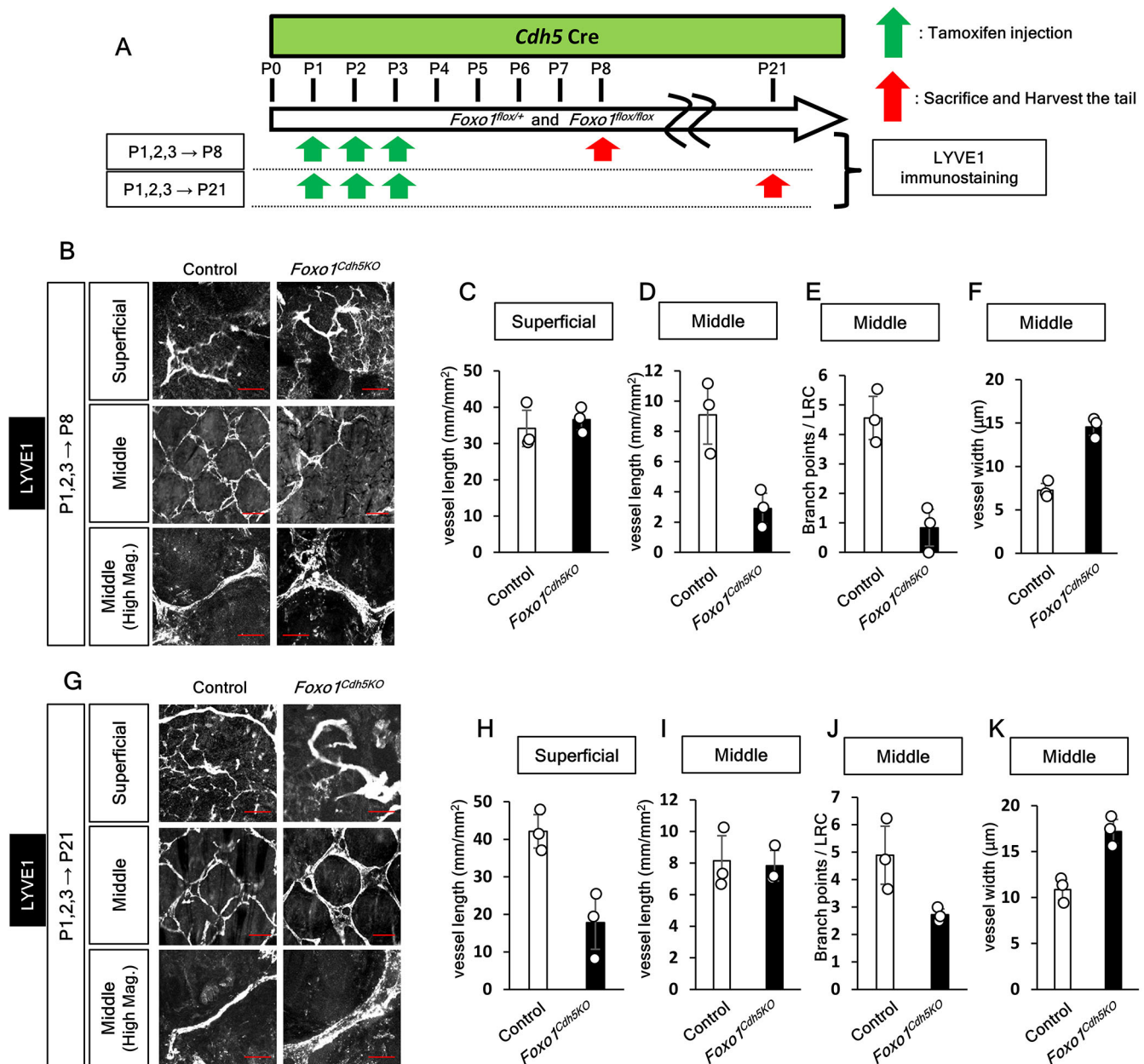


Fig. 3. Long-term abnormalities of lymphatic vasculature in *Foxo1^{Cdh5KO}* mice. (A) Schematic of tamoxifen injection for *Cdh5* promoter-dependent *Foxo1* deletion *in vivo*. (B-F) Immunostaining images of LYVE1 (gray) in control and *Foxo1^{Cdh5KO}* mice sacrificed at P8 (B). Total lymphatic vessel length based on immunostaining image for LYVE1 was measured in superficial (C) and middle (D) layers. Branch point number per LRC (E) and lymphatic vessel diameter (F) in the middle layer were also measured in P8 dermis. (G-K) Immunostaining image of LYVE1 (gray) in control and *Foxo1^{Cdh5KO}* mice sacrificed at P21 (G). Total lymphatic vessel length based on immunostaining image for LYVE1 was measured in superficial (H) and middle layer (I). Branch point number per LRC (J) and lymphatic vessel diameter (K) in the middle layer were also measured in P21 dermis; $n=3$ for control mice and $n=3$ for *Foxo1^{Cdh5KO}* mice. Scale bars: 10 μm in superficial; 20 μm in middle layer (high magnification); 50 μm in middle layer. All data are mean \pm s.d.

transfectants was lower than that observed in siNC transfectants (Fig. 8D,E), and that CXCR4 overexpression rescued the decreased migration observed in siFOXO1 transfectants (Fig. 8D,E).

***Foxo1* knockdown affected LEC proliferation and apoptosis**

We next examined the proliferative effect of CXCL12 on HDLECs in BrdU assays. Immunocytochemical staining showed that CXCL12 increased BrdU-positive HDLECs in a dose-dependent manner. This dose-dependent effect was lost and BrdU-positive cells increased in low CXCL12 levels in siFOXO1 transfected HDLECs (Fig. S11A,B). AMD3100 inhibited CXCL12-dependent

LEC proliferation in siNC transfectants, but did not inhibit the increased proliferation observed in siFOXO1 transfectants (Fig. S11A,B). The increased cell proliferation observed in FOXO1-deficient cells is generally thought to be due to a reduction of FOXO-mediated cell cycle inhibitory genes, such as *CDKN1A*, *CDKN1B*, *CDKN2A*, *CDKN2B*, *RBL2* and *GADD45A* (Bouchard et al., 2007; Furukawa-Hibi et al., 2002; Katayama et al., 2008; Kops et al., 2002; Medema et al., 2000; Nakamura et al., 2000; Seoane et al., 2004; Tran et al., 2002). To investigate their expression, qRT-PCR analysis targeting these genes was performed. Interestingly, among the cell-cycle inhibitory genes

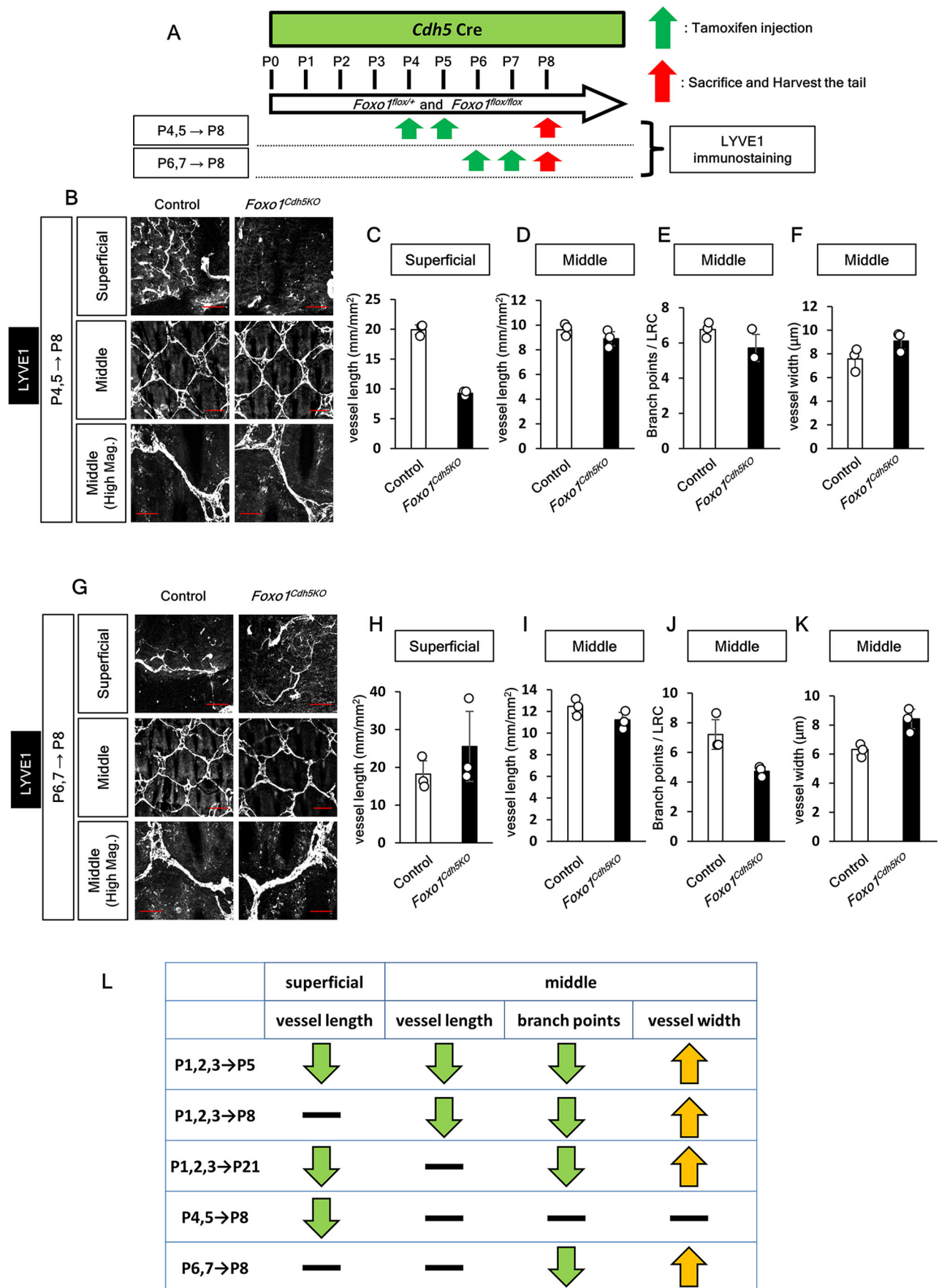


Fig. 4. See next page for legend.

Fig. 4. A different period for *Foxo1* deletion partially altered developmental lymphangiogenesis. (A) Schematic of tamoxifen injection for *Cdh5* promoter-dependent *Foxo1* deletion *in vivo*. (B-F) Immunostaining image of LYVE1 (gray) in P8 control and *Foxo1^{Cdh5KO}* mice treated with tamoxifen at P4 and P5 (B). Total lymphatic vessel length based on immunostaining image for LYVE1 was measured in superficial (C) and middle (D) layers. Branch point number per LRC (E) and lymphatic vessel diameter (F) in the middle layer were also measured in the P8 dermis. (G-K) Immunostaining image of LYVE1 (gray) in P8 control and *Foxo1^{Cdh5KO}* mice treated with tamoxifen at P6 and P7 (G). Total lymphatic vessel length based on immunostaining image for LYVE1 was measured in the superficial (H) and middle (I) layers. Branch point number per LRC (J) and lymphatic vessel diameter (K) in middle layer were also measured in the P8 dermis. (L) Summary of the abnormalities of lymphatic vasculature observed in *Foxo1^{Cdh5KO}* mice, as shown in Figs S2-S4. Scale bars: 10 μ m in superficial layer; 20 μ m in middle layer (high magnification); 50 μ m in middle layer. All data are mean \pm s.d.

we analyzed, only *CDKN2B* was downregulated in siFOXO1 transfected HDLECs (Fig. S11C). We next investigated the reduction of *CDKN2B* in *Foxo1*-deficient dermal lymphatic vessels. Anti-*CDKN2B* immunohistochemical studies in control and *Foxo1^{Cdh5KO}* dermis shows that *CDKN2B* is downregulated in *Foxo1^{Cdh5KO}* lymphatic vasculature compared with control mice (Fig. S11D,E). These results agreed with the increased cell proliferation in the dermal lymphatic vasculature in KO pups. We next investigated the mechanism of reduced apoptotic LECs observed in *Foxo1*-deficient lymphatic vasculature. In general, reduced apoptosis in FOXO1-deficient cells is thought to be caused by reduction of pro-apoptotic proteins, such as Bim (encoded by *BCL2L11*) or FasL (encoded by *FASLG*), which are directly transcribed by FOXO (Brunet et al., 1999; Dijkers et al., 2000; Gilley et al., 2003; Stahl et al., 2002). We investigated the mRNA expression of *BCL2L11* and *FASLG* in siFOXO1 transfected HDLECs compared with siNC transfectants. We observed no *FASLG* expression in HDLECs (data not shown). *BCL2L11* expression was decreased in siFOXO1 transfected HDLECs compared with siNC transfectants (Fig. S11F). We next performed immunohistochemistry with anti-Bim antibody on the tail dermis of control and *Foxo1^{Cdh5KO}* mice. We found that Bim was expressed in lymphatic capillaries in P5 control dermis, but drastically downregulated in P5 *Foxo1^{Cdh5KO}* dermis (Fig. S11G,H).

CXCR4 blockage disturbed developing lymphangiogenesis *in vivo*

We next examined the effect of CXCR4 blockage in the developing tail dermis. Scratched wild-type tails were immersed in 2 mM AMD3100 solution daily from P1 to P4 and tail dermises were subsequently harvested at P5 and used for immunohistochemistry (Fig. 9A). Tails were scratched to allow for efficient permeation of AMD3100. To check the permeation of AMD3100 into the dermis, we performed anti-CXCR4 immunohistochemical staining in tail dermises that were not treated with PP. AMD3100 treatment allowed us to detect CXCR4 without PP treatment (Fig. 9B), which meant efficient CXCR4 inactivation. Immunohistochemical studies using anti-LYVE1 antibodies showed decreased lymphatic vessel length in superficial and middle layers, but not in the deep layer in AMD3100-treated tail dermis compared with vehicle control-treated dermis (Fig. 9C-F). In the middle layer of AMD3100-treated dermis, LRC and its complexities were decreased compared with the vehicle control (Fig. 9C,G,H). However, lymphatic vessel width in the middle layer of AMD3100-treated dermis was not altered compared with vehicle control (Fig. 9C,I).

DISCUSSION

Failure to form normal connected lymphatic vasculature, as presently occurs in the *Foxo1*-deficient pups, is likely caused by impaired LEC sprouting and migration, which is essential for normal lymphatic network formation (James et al., 2013). Similar developmental lymphangiogenesis abnormalities in the tail dermis have been previously reported in mice with blocked signaling of Notch1-Dll4, ALK1 or VEGFR3 (Niessen et al., 2011, 2014). We identified downregulation of Bim and *CDKN2B* in *Foxo1*-deficient LECs as possible causes of dilation of lymphatic vessels in lymphatic *Foxo1*-deficient pups. However, Wilhelm et al. (2016) recently reported that endothelial FOXO1 works as a gatekeeper of endothelial quiescence to suppress excess growth and proliferation of endothelial cells by inhibiting MYC protein. Our qPCR analysis detected a slight increase of the *MYC* in FOXO1-depleted HDLECs (data not shown). Therefore, Myc upregulation might be one cause of the excess proliferation observed in *Foxo1*-deficient lymphatic vessels. Alternatively, the data concerning BrdU incorporation in HDLECs (Fig. S11A,B) suggest that FOXO1-deficient LECs lose control of cell proliferation due to addition of exogenous CXCL12. This might be partly attributable to the downregulation of *CDKN2B*, which induces G1 arrest. Dilation of lymphatic vessels was reported in the dorsal skin of *Foxc1^{-/-}*, *Foxc2^{-/-}*, *Tgfb1^{-/-}* and *Tgfb2^{-/-}* mice (Fatima et al., 2016; James et al., 2013). However, *Foxc1^{-/-}* and *Foxc2^{-/-}* mice do not have decreased numbers of lymphatic branch points, and *Tgfb1^{-/-}* and *Tgfb2^{-/-}* mice do not have decreased numbers of apoptotic cells in their lymphatic vessels. In this respect, the phenotypes observed in *Foxo1*-deficient lymphatic vasculature are likely due to primary effects. The same phenotypes observed presently between the three different Cre-mediated deletions of FOXO1 and minor blood vessel abnormalities in these KO pups also strongly suggest that lymphatic malformation in endothelial *Foxo1*-deficient mice primarily arise from LEC abnormalities. Altered blood vessel formation was evident only in the superficial layer of *Foxo1^{Tie2KO}* and *Foxo1^{Cdh5KO}* dermis, consistent with strong FOXO1 localization in superficial blood vessels, but not in middle and deep blood vessels of P1 and P3 dermis (Fig. 1C,D, Fig. S1C,D).

Interestingly, we observed different survival ratios of *Foxo1^{Tie2KO}*, *Foxo1^{Cdh5KO}* and *Foxo1^{Prox1KO}* mice (Fig. 2, Figs S2 and S7). Conventional and constitutive Tie2-Cre mediated deletion of *Foxo1* are reportedly lethal in the middle embryonic period (Furuyama et al., 2004; Wilhelm et al., 2016). Wilhelm et al. also reported that mice with *Pdgfrb*-Cre mediated conditional deletion of *Foxo1* survived until at least P21. These data suggest that the death of the *Foxo1^{Tie2KO}* pups was due to non-endothelial abnormalities, such as hematopoietic or endocardial malformation. Considering that *Foxo1^{Prox1KO}* pups did not die, the death of *Foxo1^{Cdh5KO}* pups was likely due to blood vessel abnormalities, except for skin tissue. The detailed cause of death requires further study.

Long-term data of *Foxo1^{Cdh5KO}* mice at P8 or P21 (Fig. 3) suggest that FOXO1 is necessary for sprouting and migration of LECs from the middle layer to the superficial layer, and suggest that other FOXO1-independent pathways might compensate for the aforementioned sprouting and migration of LECs between P5 and P8. Reduced superficial lymphatic vessels in P21 KO dermis indicates that FOXO1 is required to maintain superficial capillaries. Moreover, the results of our later inactivation analysis in *Foxo1^{Cdh5KO}* mice (Fig. 4) suggest that lymphatic vessels in the middle layer undergo development until P3, and that superficial lymphatic vessels undergo FOXO1-dependent development from

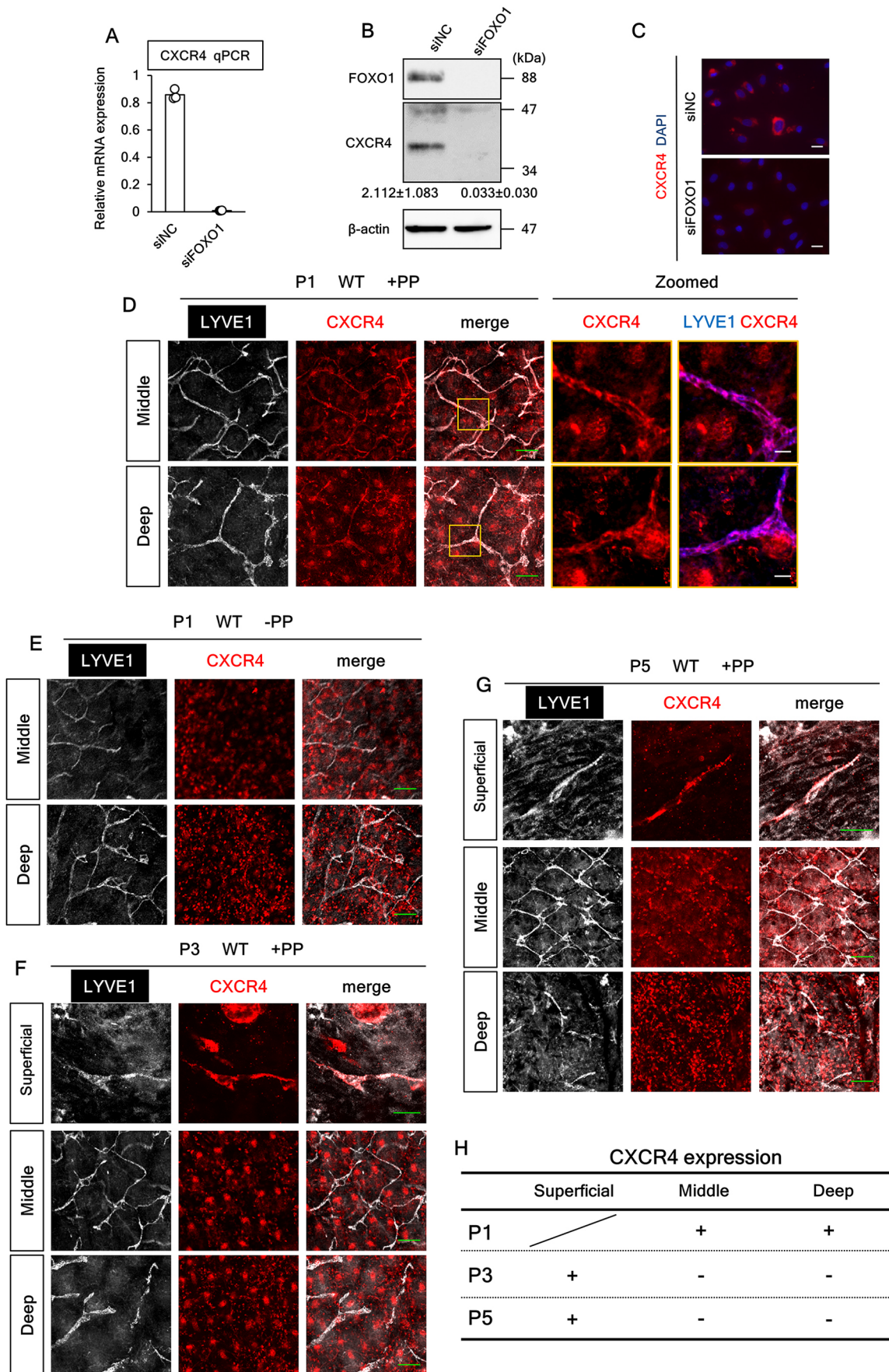


Fig. 5. See next page for legend.

Fig. 5. CXCR4 expression in lymphatic vasculature of developing tail dermis. (A) qRT-PCR analyses of HDLECs transfected with siNC or siFOXO1. $n=3$ experiments; data are mean \pm s.d. (B) Western blot analyses of CXCR4 expression in HDLECs transfected with siNC or siFOXO1. Relative band intensities of CXCR4 to β -actin are shown as mean \pm s.d. (C) Immunostaining image of CXCR4 (red) in HDLECs transfected with siNC or siFOXO1 *in vitro*. Scale bars: 20 μ m. (D-G) Immunostaining image showing CXCR4 (red) and LYVE1 (gray) expression in wild-type dermal lymphatic capillaries in each dermal layer at P1 (D,E), P3 (F) and P5 (G) stage incubated with or without protein phosphatase (PP). The areas outlined with yellow boxes in D are shown in more detail in the two right panels. (H) Lymphatic CXCR4 localization pattern in each dermal layer at P1, P3 and P5. Expression in lymphatic endothelium: + and – indicate expression and no expression in lymphatic endothelium, respectively. Scale bars: 8 μ m in G (superficial layer); 10 μ m in D (zoomed images) and F (superficial layer); 50 μ m in middle and deep layers in D-G.

P4 to P5. These results also indicate the completion of sprouting and migration of LECs from the middle to the superficial layer by P5. However, we cannot explain the different phenotypes in the middle lymphatic capillaries between the P4 to P5 treatment and the P6 to P7 treatment. As one possibility, the different duration of *Foxo1* deficit (4 days in the P4, P5-P8 regimen and 2 days in the P6, P7-P8 regimen) might affect the downstream gene profile of FOXO1.

Our findings potentially implicate CXCR4 downregulation in impaired developmental lymphangiogenesis in *Foxo1*-deficient mice. CXCR4 expression in the endothelial cells of normal mammalian tissues may be limited in blood vessels, especially in the arteries. CXCR4 protein is reportedly expressed in blood capillaries, but not in lymphatic capillaries during inflammation-related vasculogenesis in the mouse ear dermis (Zraggen et al., 2014). However, CXCR4 was expressed in the trunk lymphatic vessel of developing zebrafish, with limited localization and time-frame for expression (Cha et al., 2012), and in lymphatic vessels growing into a Matrigel plug containing VEGFC and in the tumor-associated lymph node and melanoma tissue (Zhuo et al., 2012). These data suggest that CXCR4 is expressed in lymphatic vessels under tightly regulated conditions, such as peripheral cytokine concentrations. These findings are consistent with our findings that CXCR4 expression in developing dermal lymphatic capillaries was very transient and localized, indicating that CXCR4 is expressed in lymphatic capillaries that are still developing, and not in fully formed lymphatic vessels. The lack of alteration in mesenteric lymphatic vessels in *Foxo1^{Cdh5KO}* pups (Fig. S5) is evidence that lymphangiogenic regulation by FOXO1-CXCR4 is tissue and time specific. We also found abnormalities in (pre-) collecting lymphatic vessels in *Foxo1^{Cdh5KO}* pups (Fig. S4). Because we did not detect CXCR4 in collecting lymphatics (data not shown), this phenotype seems not to be attributable to the downregulation of CXCR4. This is consistent with the lack of reduction in collecting vascular length (Fig. S4B).

CXCL12 is expressed in the epidermis, papillary dermis, blood vessels, nerve tissues, sweat glands and hair follicles of adult rat skin (Avniel et al., 2006). CXCL12 was also localized in LYVE1-positive dermal lymphatic endothelium in a 2,4-dinitro-1-fluorobenzene-induced contact dermatitis mice model (Kabashima et al., 2007). However, it is unlikely that LEC-derived autocrine CXCL12 induces the migration of LECs because of the non-concomitant expression of CXCR4 and CXCL12 in the LECs of the same layer. Moreover, chemoattraction between the LECs of the two different layers is also unlikely because the pattern of CXCR4/CXCL12 expression (CXCL12 in the middle LECs and CXCR4 in the superficial LECs) does not match the direction of

chemoattraction. Another source of CXCL12 for LEC migration likely exists. As CXCL12 is a secreted protein, *in situ* hybridization could be suitable to detect this elusive CXCL12 source.

Among other FOX transcription factors, FOXC1 and FOXC2 increase *Cxcr4* expression in mouse embryonic endothelial cells (Hayashi and Kume, 2008). FOXC1 and FOXC2 are regulate developmental lymphangiogenesis in embryonic mice (Fatima et al., 2016). Moreover, FOXO3a binds to the promoter region of the *CXCR4* gene in prostate cancer cells (Dubrovskaya et al., 2012). In this study, qRT-PCR demonstrated that *FOXO1* knockdown did not induce *FOXC1/2* or *FOXO3A* downregulation (data not shown), suggesting that CXCR4 downregulation caused by *FOXO1* knockdown is a primary effect.

Consistent with the migration assay results (Fig. 8), a previous study has reported that murine primary LECs migrate toward CXCL12 supplied at 1 to 100 ng ml⁻¹ (Zhuo et al., 2012). Other studies have demonstrated that various CXCR4-positive cells, including lymphocytes, hematopoietic cells, malignant tumor cells, endothelial cells and epithelial cells, migrate toward CXCL12 at approximately the same concentrations (Fernandis et al., 2003, 2004; Mirshahi et al., 2000; Wuchter et al., 2014; Yokohama-Tamaki et al., 2015). Furthermore, the impaired lymphangiogenesis in postnatal tail dermis treated with CXCR4 antagonist strongly suggests that impaired lymphangiogenesis in the tail dermis of *Foxo1*-deficient mice is attributable, in part, to the downregulation of the CXCR4 protein in LECs, followed by inhibition of cell migration towards the surrounding CXCL12 gradient. Interestingly, CXCR4 blockage in the developing tail dermis did not alter lymphatic vessel width, unlike the *Foxo1*-deficient tail dermis. This indicates that dilated lymphatic vessels in *Foxo1*-deficient tail are not completely due to attenuated CXCL12-CXCR4 signaling, but instead to decreased FOXO1 and its other target genes.

The present data suggest that FOXO1 KO in LECs decreases migration toward CXCL12 by downregulating CXCR4 (Fig. 10). FOXO1 KO induces excess LEC proliferation and decreased LEC apoptosis (Fig. 10). This results in a disconnected and dilated structure of the lymphatic vasculature in endothelial *Foxo1*-deficient mouse-tail dermis (Fig. 10). Increased proliferation and decreased apoptosis in FOXO1-deficient LECs might be caused by the reduction of CDKN2B and Bim (Fig. 10). However, CDKN2B and Bim are two of various possibilities. Furthermore, the roles that FOXO1 serve in physiological lymphangiogenesis during early embryonic development and in pathological lymphangiogenesis during inflammation or tumor cell recruitment, as that observed in the tail dermis, remain unknown. Inhibition of CXCR4/CXCL12 signaling suppresses corneal inflammatory lymphangiogenesis (Du and Liu, 2016). Future studies to elucidate the involvement of FOXO1 in pathological lymphangiogenesis would clarify the utility of this protein as a potent therapeutic target.

MATERIALS AND METHODS

Animals

The production of C57BL/6-*Foxo1^{flox/flox}* and C57BL/6-*Foxo1^{flox/+}* mice was as previously described (Miyazaki et al., 2012). *Tie2-CreER^{T2}* C57BL/6 mice showing endothelial cell-specific tamoxifen-inducible Cre recombinase expression (Forde et al., 2002) were kindly provided by Dr Bernd Arnold (German Cancer Research Center, Heidelberg, Germany). *Tie2-Cre ER^{T2}-Foxo1^{flox/flox}* mice and *Tie2-Cre ER^{T2}-Foxo1^{flox/+}* mice were used for experiments. The *Cre* genotype was determined by PCR using the primer set shown in Table S4 and *flox* phenotypes were determined as previously described (Miyazaki et al., 2012). Tamoxifen (Sigma-Aldrich) dissolved in peanut oil (Sigma-Aldrich) was intraperitoneally injected

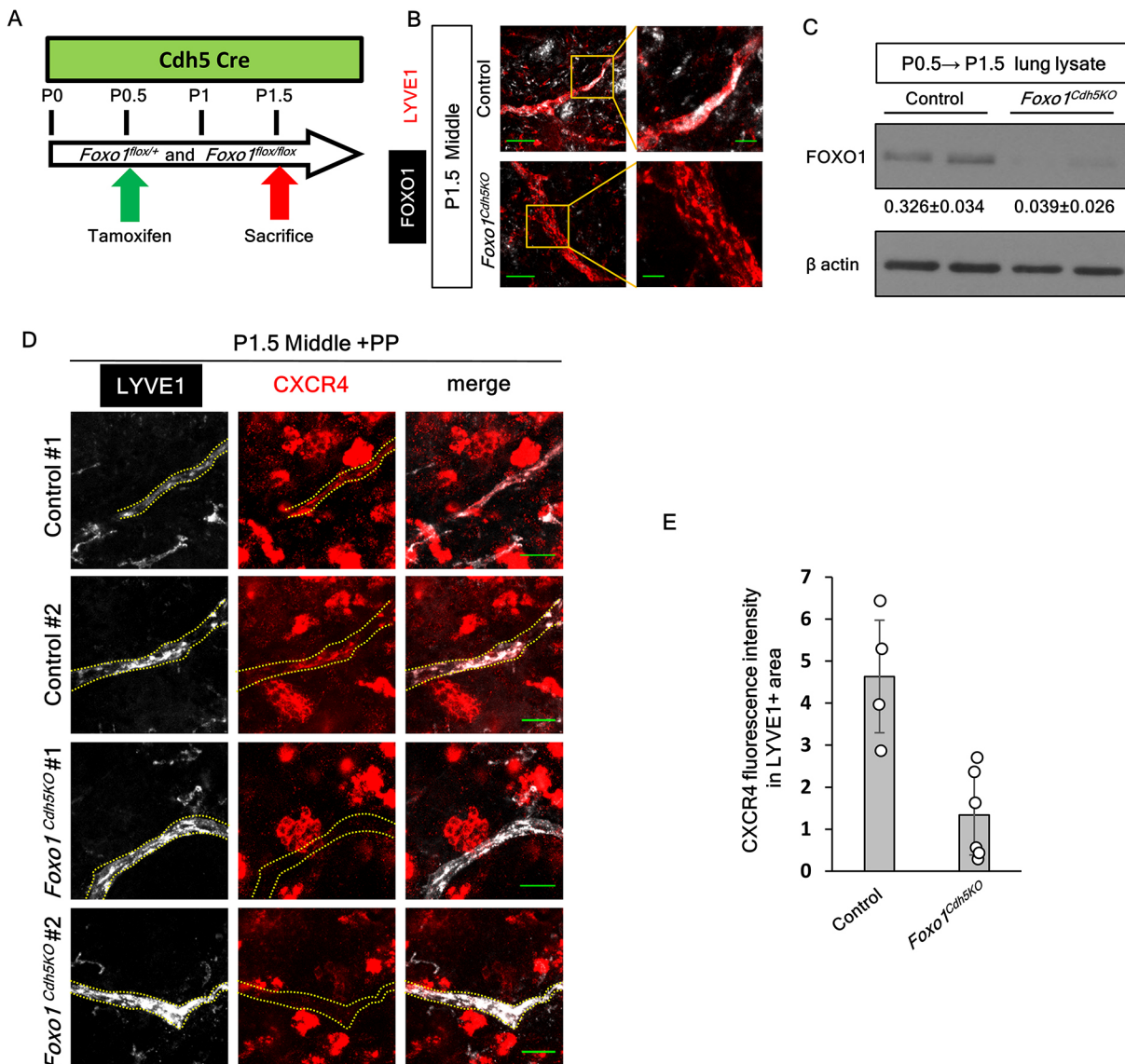


Fig. 6. *Foxo1* KO reduced CXCR4 expression in developing tail dermis. (A) Schedule of tamoxifen injection and dermis harvest to investigate CXCR4 reduction in *Foxo1*-deficient lymphatic vasculature. (B) Anti-FOXO1 and anti-LYVE1 immunohistochemistry in the P1.5 control and *Foxo1^{Cdh5KO}* dermis. (C) Anti-FOXO1 western blot analysis of lung lysate from P1.5 control and *Foxo1^{Cdh5KO}* mice. Relative band intensities of FOXO1 compared with β -actin are shown as mean \pm s.d. (D) Immunostaining images showing CXCR4 (red) and LYVE1 (gray) expression in control and *Foxo1^{Cdh5KO}* mouse dermal lymphatic capillaries incubated with PP at P1.5. (E) Quantification of CXCR4-positive fluorescence intensity in lymphatic vessels shown in D. Four (control) and six (KO) microscopic fields from three pups each were assessed. Analyzed vessel area is \sim 150–300 μm^2 per field. Data are mean \pm s.d. Scale bars: 20 μm in B (low magnification) and D; 5 μm in B (high magnification).

(50 $\mu\text{g/g}$ body weight) into *Tie2-Cre ER^{T2}-Foxo1^{fllox/fllox}* and *Tie2-Cre ER^{T2}-Foxo1^{fllox/+}* mice at the indicated time point to specifically delete *Foxo1* in endothelial cells. The production of *Cdh5-Cre ER^{T2}* mice is as previously reported (Okabe et al., 2014). *Cdh5-Cre ER^{T2}-Foxo1^{fllox/fllox}* mice and *Cdh5-Cre ER^{T2}-Foxo1^{fllox/+}* mice were used for experiments. The production of *Prox1-Cre ER^{T2}* mice is as previously reported (Bazigou et al., 2011). *Prox1-Cre ER^{T2}-Foxo1^{fllox/fllox}* mice and *Prox1-Cre ER^{T2}-Foxo1^{fllox/+}* mice were used for experiments. All the animal experiments were approved by The Osaka University Graduate School of Medicine Intramural Animal Care and Use Committee or The Kagawa Prefectural University of Health Sciences Institutional Animal Care and Use Committee. We used as few animals as possible and took steps to minimize their suffering.

Isolation of whole-tail dermis from mice

Mouse-tail dermis was harvested as described previously (Niessen et al., 2014), cut to 3 mm in width and fixed in 100% methanol at -20°C .

Administration of BrdU to detect proliferating cells in mouse tissues

Saline solution containing BrdU (Wako, Japan) was intraperitoneally injected into mice (50 $\mu\text{g/g}$ body weight) at P5 1 h before they were sacrificed.

AMD3100 treatment of mouse tail

The tails of wild-type C57BL/6 mice were scratched with a needle at P1 and immersed in PBS containing 50% DMSO (vehicle) or 2 mM AMD3100 from P1 to P4 daily and harvested at P5. The purpose of this scratching was to allow for efficient permeation of AMD3100 and not to induce pathological lymphangiogenesis. The efficient CXCR4 antagonism in this method was confirmed (Fig. 9B). Only one streaky scratch was made on the dorsal side of tail down to the depth of the epidermis. The duration of exposure was 5 min. Immunohistochemical studies were performed only on the ventral side of tail dermis to avoid the influence of pathological conditions.

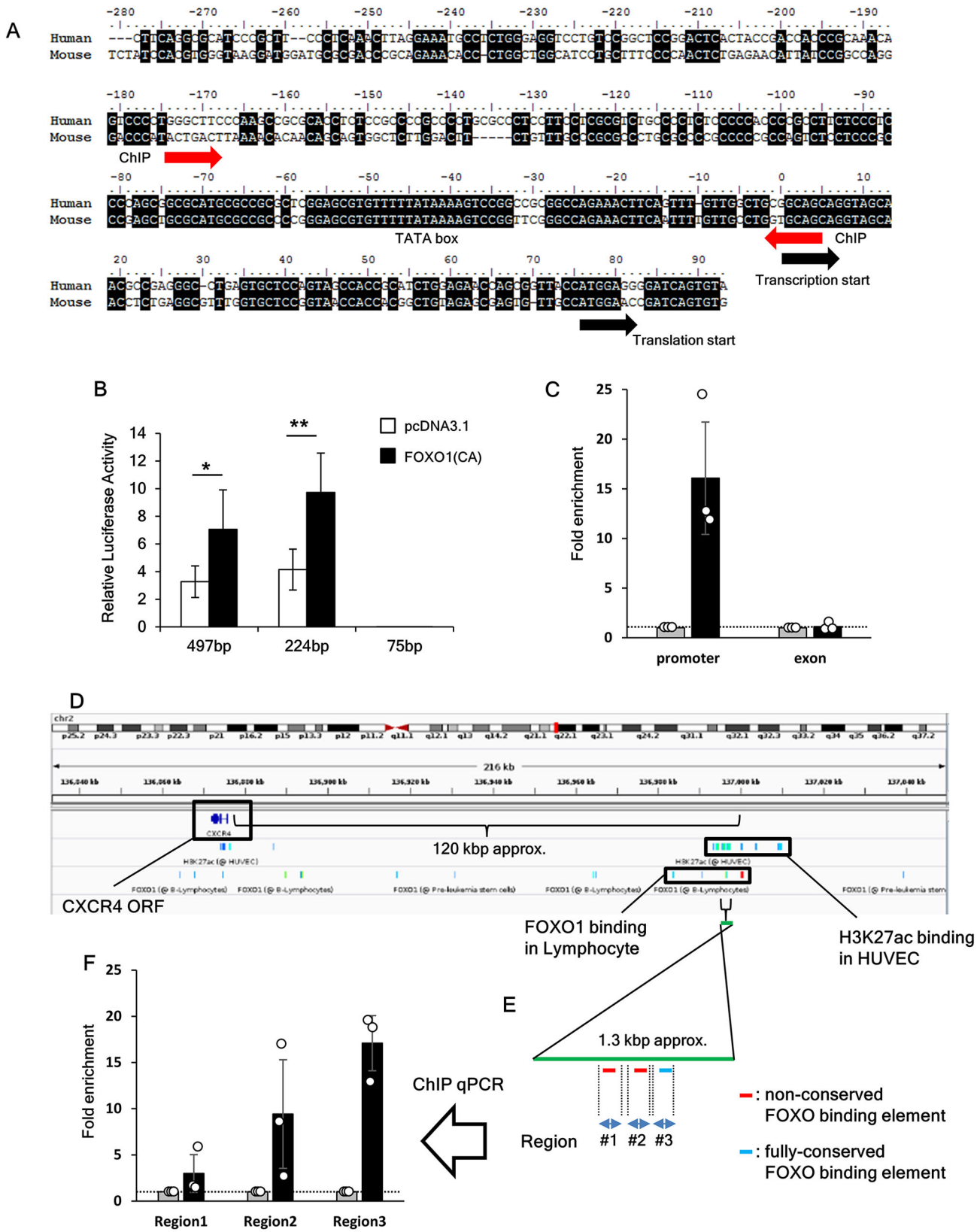


Fig. 7. See next page for legend.

Immunohistochemistry

Tissues were pre-incubated with 1 M hydrochloric acid (Sigma-Aldrich) for 1 h at 37°C to detect BrdU. The whole tail dermis was washed, blocked with

blocking reagent (Perkin Elmer) and incubated with the primary antibodies shown in Table S3. To detect total CXCR4 protein using the UMB2 antibody (Abcam), the whole-tail dermis was incubated with 800 U Lambda

Fig. 7. CXCR4 is a direct transcriptional target of FOXO1. (A) Alignment of human and mouse *Cxcr4* promoter regions. Red arrows indicate the ChIP primers shown in C. (B) Luciferase reporter assay using constructs with various lengths of the murine genomic *Cxcr4* region upstream of the start codon, which were co-transfected with FOXO1(CA) vector. The results are the mean \pm s.d. from five experiments; * P <0.05, ** P <0.01. (C) ChIP qPCR analysis using HDLECs and an anti-FOXO1 antibody. The promoter region shown in A was amplified by PCR. Exon 2 of CXCR4 was used as a negative control. Data are fold enrichment over isotype IgG control. The results are the mean \pm s.d. from three experiments. (D) Functional promoter and enhancer of the *CXCR4* gene gained from ENCODE ChIP-seq database. (E) Schematic depiction of the *CXCR4* enhancer region containing three different FBEs. (F) ChIP qPCR analysis using HDLECs and an anti-FOXO1 antibody. Three enhancer regions shown in E, each containing one FBE, were amplified by PCR. Data are mean fold enrichment over isotype IgG control \pm s.d. n =3 experiments.

Protein Phosphatase (New England Biolabs) for 1.5 h at 32°C before blocking. After incubation with the primary antibodies, the tissues were washed and incubated with the secondary antibodies (Table S3) and subsequently washed and mounted. All tissues were observed by confocal laser scanning microscopy (Olympus).

Cell culture

HDLECs were purchased from PromoCell (Germany) and cultured in a 5% CO₂ atmosphere at 37°C, using medium from the Endothelial Basal Medium MV2 Kit (PromoCell) supplemented with 5% FCS. HDLECs from passage 5 were used for all experiments. The HDLEC we purchased

originated from the juvenile foreskins of individual donors. All *in vitro* analysis was performed using HDLECs from two different donors and confirmed only minor variation between these. HeLa cells were cultured in DMEM containing 10% FBS in a 5% CO₂ atmosphere.

In vitro transfection of siRNA and the AAV vector

Specific siRNAs against human *FOXO1* (siGENOME human FOXO1 Smart Pool 2308) and a random siRNA as a negative control (non-targeting siRNA#3) were purchased from Thermo Fisher Scientific. The final additive concentration of siRNA was 0.2 nM, which is low enough to limit off-target effects of siRNA. All siRNAs were transfected using the Lipofectamine RNAiMAX reagent (Invitrogen). AAV-EGFP and AAV-CXCR4 vector plasmid were produced using AAVpro Helper Free System (AAV6) (Takara Bio, Japan), transfected in HEK293T (AAVpro 293T cell line, Takara Bio, Japan) and purified with AAVpro purification kit (Takara Bio, Japan). We used the AAV vector at 1:1000 dilution.

cDNA microarray

A cDNA microarray study was performed using cDNA from HDLECs transfected with siFOXO1 or siNC RNA for 72 h. The array was examined by Takara Bio (Japan) using the Agilent Expression Array service.

Reagents

Human recombinant SDF1 α (CXCL12) was purchased from Peprotech and dissolved in 0.1% BSA to a final concentration of 100 ng μ l⁻¹. AMD3100, a specific antagonist of CXCR4, was purchased from Sigma-Aldrich and

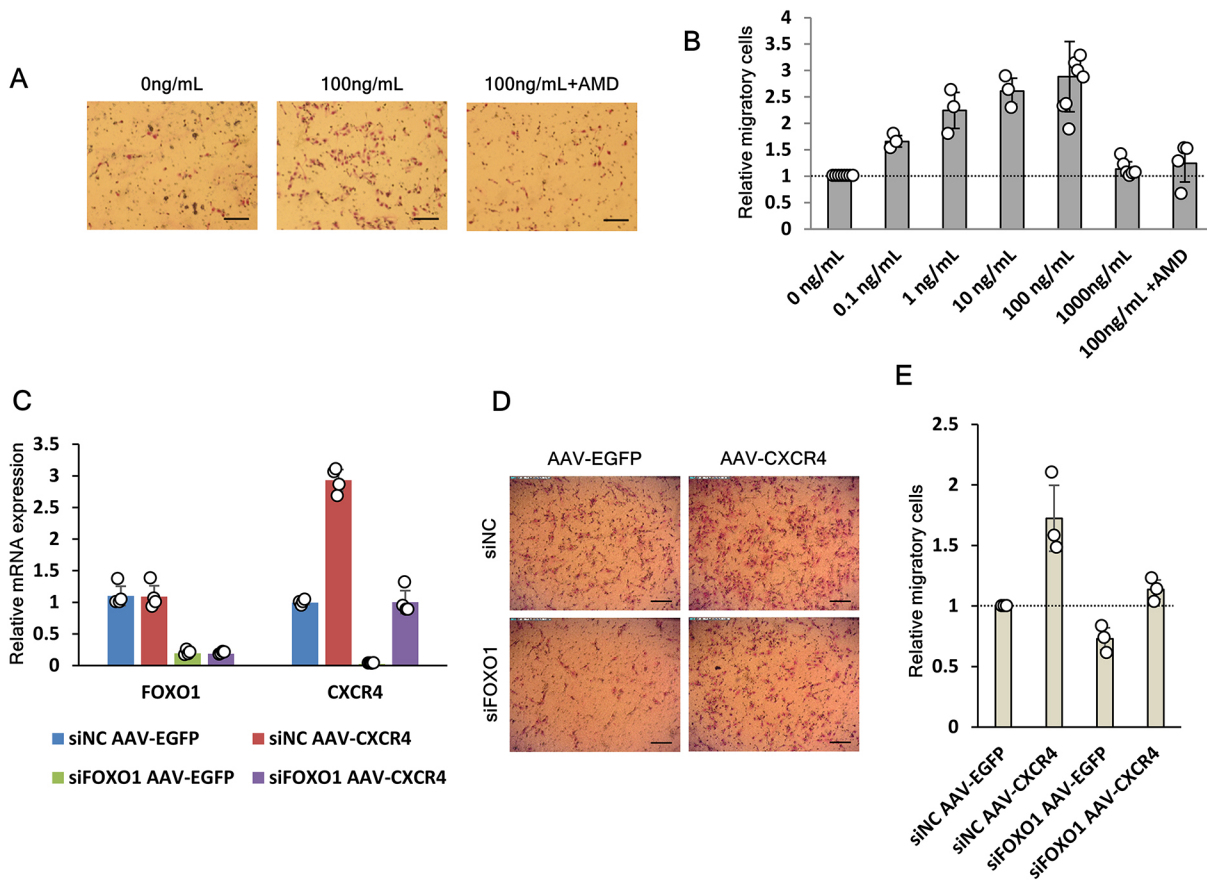


Fig. 8. FOXO1 knockdown reduced migration toward CXCL12 by CXCR4 reduction. (A) Giemsa-stained basolateral side of transwell membranes following transwell migration toward 100 ng ml⁻¹ CXCL12. AMD: AMD3100 (CXCR4 antagonist). (B) Relative migratory cell count following Giemsa staining of the basolateral side of transwell membranes, following a 5.5 h transwell migration toward various concentrations of CXCL12. (C) qRT-PCR analysis of HDLEC transfected with siNC or siFOXO1 and AAV-EGFP or AAV-CXCR4; n =4 experiments; data are mean \pm s.d. (D) Giemsa-stained transwell membranes after a 5.5 h migration of HDLECs transfectants toward 100 ng ml⁻¹ CXCL12; HDLECs were transfected with siNC or siFOXO1 and AAV-EGFP or AAV-CXCR4. (E) Migratory cell counts for the experiments described in D. Data are mean \pm s.d. n =3 experiments. Scale bars: 100 μ m.

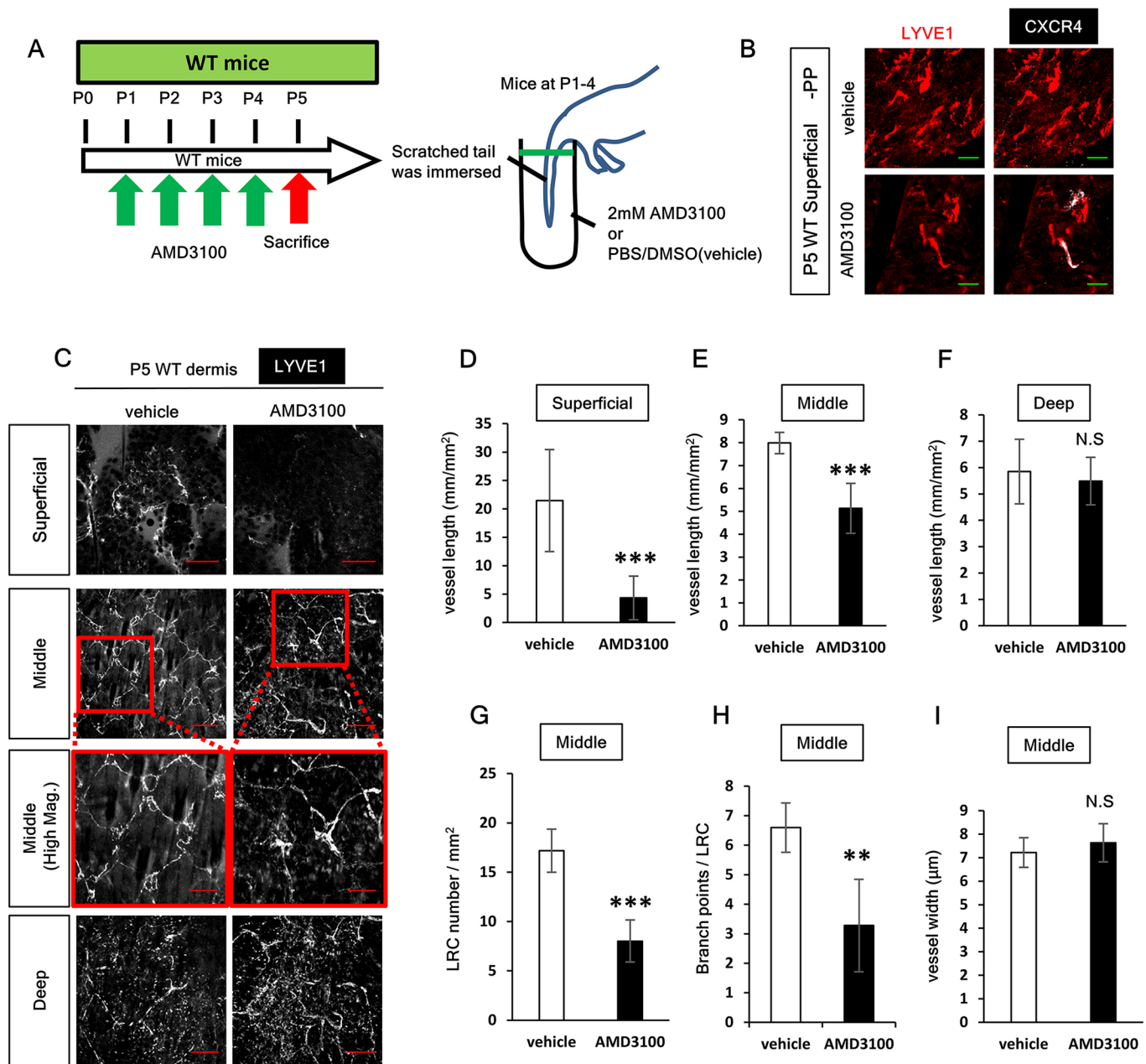


Fig. 9. CXCR4 blockage in developing tail dermis impaired lymphatic vessel formation. (A) Schematic image of CXCR4 *in vivo* blockage experiment. Wild-type tail was scratched with a needle and immersed in 2 mM AMD3100 each day, from P1 to P4, and harvested at P5 for the immunohistochemistry study. (B) Anti-CXCR4 and anti-LYVE1 immunohistochemistry study in the P5 dermis harvested as described in A without PP treatment. Scale bars: 5 µm. (C) Immunostaining image of LYVE1 in each layer of the tail dermis of P5 wild-type mice harvested as indicated in A. Scale bars: 100 µm in middle and deep layer; 50 µm in middle layer (high magnification); 20 µm in the superficial layer. (D-F) Quantification of LYVE1-positive vessel length per microscopic field area in superficial (D), middle (E) and deep (F) layers of AMD3100-treated tail dermis or vehicle control. (G-I) Quantification of LRC number per microscopic field area (G), branch point number per LRC (H) and LYVE1-positive vessel width (I) in P5 tail dermis of AMD3100-treated tail dermis or vehicle control; $n=6$ vehicle-treated mice and 5 AMD3100-treated mice. Data are mean \pm s.d. ** $P<0.01$, *** $P<0.001$. vs, vehicle; N.S., not significant.

dissolved in distilled water to a final concentration of 20 mM. The final additive concentration of AMD3100 was 5 µM.

Immunocytochemistry

After various treatments, HDLECs were fixed with 4% paraformaldehyde (PFA). To detect BrdU, cells were incubated in 1 M hydrochloric acid for 20 min at 37°C. Cells were then treated with 0.5% (v/v) Triton X-100, blocked with BSA (Sigma-Aldrich), and subsequently incubated with the appropriate primary antibody (Table S3), washed and incubated with the appropriate secondary antibody (Table S3). After washing, cells were

treated with DAPI (Sigma-Aldrich) and mounted. Slides were observed by fluorescence microscopy (BX53-34-FL-2, Olympus). To detect CXCR4 expression, cells were incubated with primary antibody before fixation with 4% PFA.

Western blot analysis

HDLECs were lysed in the buffer containing 2% SDS and protease/phosphatase inhibitor cocktail (Nacalai Tesque, Japan). Cell lysates were subjected to SDS-PAGE and transferred to a PVDF membrane (Millipore, USA). The membrane was blocked with 3% skim milk and incubated with

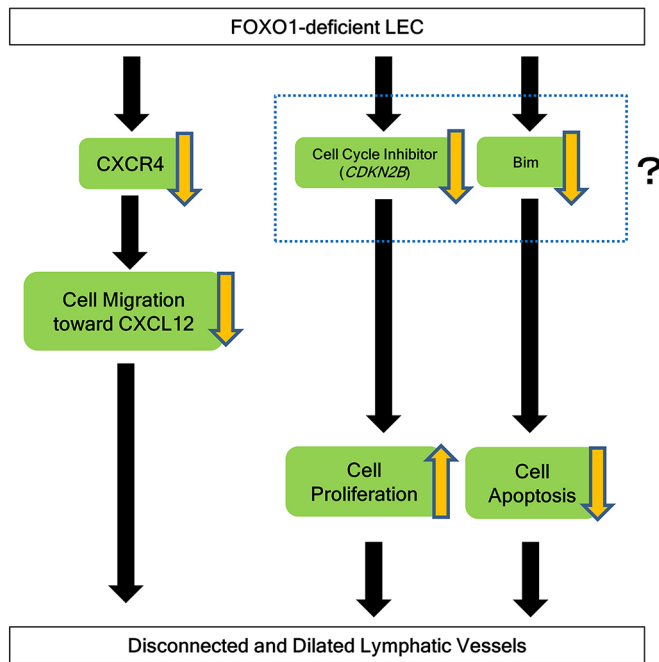


Fig. 10. Schematic representation of a model integrating our results.

Schematic image of the influence of FOXO1 deficit on LEC migration toward CXCL12, LEC proliferation and LEC apoptosis. FOXO1-deficient LECs exhibit decreased migratory activity toward exogenous CXCL12 because of CXCR4 downregulation. Meanwhile, in FOXO1-deficient LECs, levels of the cell cycle inhibitor CDKN2B are decreased, resulting in excess LEC proliferation. Moreover, the pro-apoptotic regulator Bim is decreased and thus apoptosis is suppressed in *Foxo1*-deficient LECs. These anti-migratory, proliferation-promoting and anti-apoptotic activities in *Foxo1*-deficient LECs are thought to lead to the disconnected and dilated lymphatic vasculature observed in the tail dermis of *Foxo1*-deficient mice.

the appropriate primary antibody (Table S3). After washing, the membrane was incubated with the appropriate secondary antibody (Table S3). The membrane was developed using the ECL detection system (GE Health Care) or X-ray film.

Isolation of total RNA and qRT-PCR

Total RNA was harvested from HDLECs with RNA ISO (Takara Bio, Japan). Subsequently, cDNA was synthesized with reverse transcriptase (ReverTraAce with gDNA remover, TOYOBO, Japan) and qPCR was performed using the THUNDERBIRD qPCR Mix (TOYOBO, Japan) in the CFX Connect Real-Time System (Bio-Rad) or StepOnePlus Real-Time System (Applied Biosystems). Expression levels were normalized to *ACTB* expression. The primer sets used for qRT-PCR are shown in Table S4.

Luciferase reporter assays

The 497 bp, 224 bp and 75 bp fragments from the murine genomic CXCR4 region, upstream from the start codon, were cloned by PCR using genomic DNA from a C57BL/6J mouse. Briefly, flanking 5' XhoI and 3' HindIII sites were added during PCR, and the PCR product was digested with these restriction enzymes. Subsequently, the PCR products were inserted in the pGL4.14 vector (Promega), which was pre-digested with XhoI and HindIII. Construction of the murine FOXO1-expression vector (pcDNA3.1-FOXO1-myc-His) has been previously described (Furuyama et al., 2000). Next, 1.5×10^4 HeLa cells were transfected with 100 ng each of the reporter vector and the FOXO1-expression vector (or empty pcDNA3.1 vector), as well as 6 ng of the pGL 4.74 TK promoter-driven *Renilla* luciferase vector as a transfection control, in a 96-well plate using the Lipofectamine 2000 reagent (Invitrogen). At 24 h post-transfection, luciferase activity was measured using the Dual-Luciferase Reporter Assay System (Promega) in a chemiluminescence-scanning plate reader (Berthold Technologies).

ChIP qPCR

Eighty percent confluent HDLECs in three 10 cm dishes were fixed in 1% formalin and used for ChIP assays. ChIP assays were performed using the ChIP-IT Express kit (Active Motif) and an anti-FOXO1 antibody (1:67, Abcam, ab39670). Primers used are shown in Table S4. qPCR was performed using the THUNDERBIRD qPCR Mix (Toyobo) using StepOnePlus Real-Time System (Applied Biosystems). The data were calculated as fold enrichment compared with the isotype IgG control.

Cell-migration assay

The apical chambers of transwell plates (Falcon Cell Culture Inserts, 24-well, 8 μ m; Corning) were pre-coated with type-I collagen from rat tail (BD Biosciences). HDLECs (5.0×10^4) in serum-free medium (if necessary containing 5 μ M AMD3100) were added to the upper chamber. The lower chamber was filled with serum-free medium containing various concentrations of CXCL12 or BSA (as a control). Transwell membranes were inserted and incubated for 5.5 h at 37°C. After incubation, non-migrated cells in the apical chamber were removed, and the basolateral side of each filter was fixed with 4% PFA and subsequently Giemsa stained. Migratory cells were counted by microscopy.

Image analysis

All image analyses were performed with the analysis software for FV10i (Olympus) or ImageJ software (Abramoff et al., 2004; Schneider et al., 2012). The detailed method for measurement of lymphatic vessels are shown as Fig. S12 and its legend. Blood vessels were analyzed with the same method used for lymphatic measurement. Total blood vessel length was measured and then divided by the area of the microscopic field. We analyzed three control pups and three KO pups, with three microscopic fields per pup. BrdU-positive cells and cleaved caspase 3-positive cells were counted and divided by vessel length.

Fluorescence intensity analysis

Nuclear FOXO1 fluorescence intensity was measured with ImageJ software. Each LEC nucleus was encircled after DAPI staining and fluorescence intensity inside the surrounded regions were calculated. All LEC nuclei in a $\times 1600$ microscopic field were measured. The microscopic field with the best anti-FOXO1 immunostaining property was chosen for each sample and measured. Three wild-type pups at each stage were analyzed.

Statistical analysis

All experiments were repeated at least three times. For large sample sizes ($n \geq 5$), statistical analyses were performed with Student's *t*-test or Welch's *t*-test. $P < 0.05$ was considered to indicate a statistically significant difference. The *P* values were corrected using Bonferroni's method for multiple comparisons. For small sample sizes ($n < 5$), no statistical analysis was performed and describing whether it is a 'significant' difference or not has been avoided. Instead, an individual data plot for small sample size comparison is shown.

Acknowledgements

We thank Dr Bernd Arnold for providing *Tie2CreER* mice and Dr Tajja Mäkinen for providing *Prox1 CreER* mice.

Competing interests

The authors declare no competing or financial interests.

Author contributions

Conceptualization: T.F.; Formal analysis: K.N.; Investigation: K.N., M.K., E.S.; Resources: F.T., S.M., Y.K., J.-i.M.; Writing - original draft: K.N.; Writing - review & editing: S.I., T.F.; Supervision: M.F., S.S., T.S., S.I., T.F.; Funding acquisition: S.I., T.F.

Funding

This work was supported by Grants-in-Aid for Scientific Research from the Japan Society for the Promotion of Science (15K08142 to T.F. and 16K08442 to S.I.).

Data availability

The DNA microarray datasets generated in this study have been deposited in Gene Expression Omnibus under accession number GSE142608.

Supplementary information

Supplementary information available online at
<http://dev.biologists.org/lookup/doi/10.1242/dev.181545.supplemental>

References

- Abràmoff, M. D., Magalhães, P. J. and Ram, S. J. (2004). Image processing with ImageJ. *Biophoton. Int.* **11**, 36-43.
- Accili, D. and Arden, K. C. (2004). FoxOs at the crossroads of cellular metabolism, differentiation, and transformation. *Cell* **117**, 421-426. doi:10.1016/S0092-8674(04)00452-0
- Achen, M. G., Jeltsch, M., Kukk, E., Mäkinen, T., Vitali, A., Wilks, A. F., Alitalo, K. and Stackler, S. A. (1998). Vascular endothelial growth factor D (VEGF-D) is a ligand for the tyrosine kinases VEGF receptor 2 (Flk1) and VEGF receptor 3 (Flt4). *Proc. Natl. Acad. Sci. USA* **95**, 548-553. doi:10.1073/pnas.95.2.548
- Adams, R. H., Wilkinson, G. A., Weiss, C., Diella, F., Gale, N. W., Deutsch, U., Risau, W. and Klein, R. (1999). Roles of ephrinB ligands and EphB receptors in cardiovascular development: demarcation of arterial/venous domains, vascular morphogenesis, and sprouting angiogenesis. *Genes Dev.* **13**, 295-306. doi:10.1101/gad.13.3.295
- Avniel, S., Arik, Z., Maly, A., Sagie, A., Basst, H. B., Yahana, M. D., Weiss, I. D., Pal, B., Wald, O., Ad-El, D. et al. (2006). Involvement of the CXCL12/CXCR4 pathway in the recovery of skin following burns. *J. Invest. Dermatol.* **126**, 468-476. doi:10.1038/sj.jid.5700069
- Bazigou, E., Lyons, O. T. A., Smith, A., Venn, G. E., Cope, C., Brown, N. A. and Mäkinen, T. (2011). Genes regulating lymphangiogenesis control venous valve formation and maintenance in mice. *J. Clin. Invest.* **121**, 2984-2992. doi:10.1172/JCI58050
- Bleul, C. C., Fuhlbrigge, R. C., Casasnovas, J. M., Aiuti, A. and Springer, T. A. (1996). A highly efficacious lymphocyte chemoattractant, stromal cell-derived factor 1 (SDF-1). *J. Exp. Med.* **184**, 1101-1109. doi:10.1084/jem.184.3.1101
- Bleul, C. C., Wu, L., Hoxie, J. A., Springer, T. A. and Mackay, C. R. (1997). The HIV coreceptors CXCR4 and CCR5 are differentially expressed and regulated on human T lymphocytes. *Immunology* **94**, 1925-1930. doi:10.1073/pnas.94.5.1925
- Bouchard, C., Lee, S., Paulus-Hock, V., Loddenkemper, C., Eilers, M. and Schmitt, C. A. (2007). FoxO transcription factors suppress Myc-driven lymphomagenesis via direct activation of Arf. *Genes Dev.* **21**, 2775-2787. doi:10.1101/gad.453107
- Brunet, A., Bonni, A., Zigmond, M. J., Lin, M. Z., Juo, P., Hu, L. S., Anderson, M. J., Arden, K. C., Blenis, J. and Greenberg, M. E. (1999). Akt promotes cell survival by phosphorylating and inhibiting a forkhead transcription factor. *Cell* **96**, 857-868. doi:10.1016/S0092-8674(00)80595-4
- Cha, Y. R., Fujita, M., Butler, M., Isogai, S., Kochhan, E., Siekmann, A. F. and Weinstein, B. M. (2012). Chemokine signaling directs trunk lymphatic network formation along the preexisting blood vasculature. *Dev. Cell* **22**, 824-836. doi:10.1016/j.devcel.2012.01.011
- Dijkers, P. F., Medema, R. H., Lammers, J.-W. J., Koenderman, L. and Coffey, P. J. (2000). Expression of the pro-apoptotic Bcl-2 family member Bim is regulated by the forkhead transcription factor FKHR-L1. *Curr. Biol.* **10**, 1201-1204. doi:10.1016/S0960-9822(00)00728-4
- Du, L.-L. and Liu, P. (2016). CXCL12/CXCR4 axis regulates neovascularization and lymphangiogenesis in sutured corneas in mice. *Mol. Med. Rep.* **13**, 4987-4994. doi:10.3892/mmr.2016.5179
- Dubrovskaya, A., Elliott, J., Salamone, R. J., Teleguev, G. D., Stakhovskiy, A. E., Schepotin, I. B., Yan, F., Wang, Y., Bouchez, L. C., Kularatne, S. A. et al. (2012). CXCR4 expression in prostate cancer progenitor cells. *PLoS ONE* **7**, e31226. doi:10.1371/journal.pone.0031226
- Dumont, D. J., Jussila, L., Taipale, J., Lymboussaki, A., Mustonen, T., Pajusola, K., Breitman, M., Alitalo, K., Carmeliet, P., Shalaby, F. et al. (1998). Cardiovascular failure in mouse embryos deficient in VEGF receptor-3. *Science* **282**, 946-949. doi:10.1126/science.282.5390.946
- Eijkelenboom, A. and Burgering, B. M. T. (2013). FOXOs: signalling integrators for homeostasis maintenance. *Nat. Rev. Mol. Cell Biol.* **14**, 83-97. doi:10.1038/nrm3507
- Enholm, B., Jussila, L., Karkkainen, M. and Alitalo, K. (1998). VEGF-C: a growth factor for lymphatic and blood vascular endothelial cells. *Trends Cardiovasc. Med.* **8**, 292-297. doi:10.1016/S1050-1738(98)00026-7
- Fatima, A., Wang, Y., Uchida, Y., Norden, P., Liu, T., Culver, A., Dietz, W. H., Culver, F., Millay, M., Mukoyama, Y.-S. et al. (2016). Foxc1 and Foxc2 deletion causes abnormal lymphangiogenesis and correlates with ERK hyperactivation. *J. Clin. Invest.* **126**, 2437-2451. doi:10.1172/JCI80465
- Fernandis, A. Z., Cherla, R. P. and Ganju, R. K. (2003). Differential regulation of CXCR4-mediated T-cell chemotaxis and mitogen-activated protein kinase activation by the membrane tyrosine phosphatase, CD45. *J. Biol. Chem.* **278**, 9536-9543. doi:10.1074/jbc.M211803200
- Fernandis, A. Z., Prasad, A., Band, H., Klösel, R. and Ganju, R. K. (2004). Regulation of CXCR4-mediated chemotaxis and chemoinvasion of breast cancer cells. *Oncogene* **23**, 157-167. doi:10.1038/sj.onc.1206910
- Ferrari, G., Cook, B. D., Terushkin, V., Pintucci, G. and Mignatti, P. (2009). Transforming growth factor-beta 1 (TGF-β1) induces angiogenesis through vascular endothelial growth factor (VEGF)-mediated apoptosis. *J. Cell. Physiol.* **219**, 449-458. doi:10.1002/jcp.21706
- Forde, A., Constien, R., Gröne, H.-J., Hämmerling, G. and Arnold, B. (2002). Temporal Cre-mediated recombination exclusively in endothelial cells using Tie2 regulatory elements. *Genesis* **33**, 191-197. doi:10.1002/gene.10117
- Fukumoto, M., Kondo, K., Uni, K., Ishiguro, T., Hayashi, M., Ueda, S., Mori, I., Niimi, K., Tashiro, F., Miyazaki, S. et al. (2018). Tip-cell behavior is regulated by transcription factor FoxO1 under hypoxic conditions in developing mouse retinas. *Angiogenesis* **21**, 203-214. doi:10.1007/s10456-017-9588-z
- Furukawa-Hibi, Y., Yoshida-Araki, K., Ohta, T., Ikeda, K. and Motoyama, N. (2002). FOXO forkhead transcription factors induce G2-M checkpoint in response to oxidative stress. *J. Biol. Chem.* **277**, 26729-26732. doi:10.1074/jbc.C200256200
- Furuyama, T., Nakazawa, T., Nakano, I. and Mori, N. (2000). Identification of the differential distribution patterns of mRNAs and consensus binding sequences for mouse DAF-16 homologues. *Biochem. J.* **349**, 629-634. doi:10.1042/bj3490629
- Furuyama, T., Kitayama, K., Shimoda, Y., Ogawa, M., Sone, K., Yoshida-Araki, K., Hisatsune, H., Nishikawa, S.-I., Nakayama, K., Nakayama, K. et al. (2004). Abnormal angiogenesis in Foxo1 (Fkhr)-deficient mice. *J. Biol. Chem.* **279**, 34741-34749. doi:10.1074/jbc.M314214200
- Gilley, J., Coffey, P. J. and Ham, J. (2003). FOXO transcription factors directly activate bim gene expression and promote apoptosis in sympathetic neurons. *J. Cell Biol.* **162**, 613-622. doi:10.1083/jcb.200303026
- Hayashi, H. and Kume, T. (2008). Forkhead transcription factors regulate expression of the chemokine receptor CXCR4 in endothelial cells and CXCL12-induced cell migration. *Biochem. Biophys. Res. Commun.* **367**, 584-589. doi:10.1016/j.bbrc.2007.12.183
- Huang, H. and Tindall, D. J. (2007). Dynamic FoxO transcription factors. *J. Cell Sci.* **120**, 2479-2487. doi:10.1242/jcs.001222
- James, J. M., Nalbandian, A. and Mukoyama, Y.-S. (2013). TGFβ signaling is required for sprouting lymphangiogenesis during lymphatic network development in the skin. *Development* **140**, 3903-3914. doi:10.1242/dev.095026
- Joukov, V., Pajusola, K., Kaipainen, A., Chilov, D., Lahtinen, I., Kukk, E., Saksela, O., Kalkkinen, N. and Alitalo, K. (1996). A novel vascular endothelial growth factor, VEGF-C, is a ligand for the Flt4 (VEGFR-3) and KDR (VEGFR-2) receptor tyrosine kinases. *EMBO J.* **15**, 290-298. doi:10.1002/j.1460-2075.1996.tb00359.x
- Kabashima, K., Shiraiishi, N., Sugita, K., Mori, T., Onoue, A., Kobayashi, M., Sakabe, J.-I., Yoshiki, R., Tamamura, H., Fujii, N. et al. (2007). CXCL12-CXCR4 engagement is required for migration of cutaneous dendritic cells. *Am. J. Pathol.* **171**, 1249-1257. doi:10.2353/ajpath.2007.070225
- Karkkainen, M. J. and Petrova, T. V. (2000). Vascular endothelial growth factor receptors in the regulation of angiogenesis and lymphangiogenesis. *Oncogene* **19**, 5598-5605. doi:10.1038/sj.onc.1203855
- Karkkainen, M. J., Haiko, P., Sainio, K., Partanen, J., Taipale, J., Petrova, T. V., Jeltsch, M., Jackson, D. G., Talikka, M., Rauvala, H. et al. (2004). Vascular endothelial growth factor C is required for sprouting of the first lymphatic vessels from embryonic veins. *Nat. Immunol.* **5**, 74-80. doi:10.1038/ni1013
- Katayama, K., Nakamura, A., Sugimoto, Y., Tsuruo, T. and Fujita, N. (2008). FOXO transcription factor-dependent p15INK4b and p19INK4d expression. *Oncogene* **27**, 1677-1686. doi:10.1038/sj.onc.1210813
- Kazenwadel, J., Scott, H. S., Harvey, N. L., Kazenwadel, J., Betterman, K. L., Chong, C.-E., Stokes, P. H., Lee, Y. K., Secker, G. A., Agalarov, Y. et al. (2015). GATA2 is required for lymphatic vessel valve development and maintenance. *J. Clin. Invest.* **125**, 2979-2994. doi:10.1172/JCI78888
- Kerjaschki, D. (2014). The lymphatic vasculature revisited. *J. Clin. Invest.* **124**, 874-877. doi:10.1172/JCI74854
- Kops, G. J. P. L., Medema, R. H., Glassford, J., Essers, M. A. G., Dijkers, P. F., Coffey, P. J., Lam, E. W.-F. and Burgering, B. M. T. (2002). Control of cell cycle exit and entry by protein kinase B-regulated forkhead transcription factors. *Mol. Cell Biol.* **22**, 2025-2036. doi:10.1128/MCB.22.7.2025-2036.2002
- Krebs, L. T., Xue, Y., Norton, C. R., Shutter, J. R., Maguire, M., Sundberg, J. P., Gallahan, D., Closson, V., Kitajewski, J., Callahan, R. et al. (2000). Notch signaling is essential for vascular morphogenesis in mice. *Genes Dev.* **14**, 1343-1352.
- Kulkarni, R. M., Greenberg, J. M. and Akeson, A. L. (2009). NFATc1 regulates lymphatic endothelial development. *Mech. Dev.* **126**, 350-365. doi:10.1016/j.mod.2009.02.003
- Mäkinen, T., Veikkola, T., Mustjoki, S., Karpanen, T., Catimel, B., Nice, E. C., Wise, L., Mercer, A., Kowalski, H., Kerjaschki, D. et al. (2001). Isolated lymphatic endothelial cells transduce growth, survival and migratory signals via the VEGF-C/D receptor VEGFR-3. *EMBO J.* **20**, 4762-4773. doi:10.1093/emboj/20.17.4762
- Medema, R. H., Kops, G. J. P. L., Bos, J. L. and Burgering, B. M. T. (2000). FOX-like Forkhead transcription factors mediate cell-cycle regulation by Ras and PKB through p27kip1. *Nature* **404**, 782-787. doi:10.1038/35008115
- Mirshahi, F., Pourtau, J., Li, H., Muraine, M., Trochon, V., Legrand, E., Vannier, J.-P., Soria, J., Vasse, M. and Soria, C. (2000). SDF-1 activity on microvascular endothelial cells: consequences on angiogenesis in in vitro and in vivo models. *Thromb. Res.* **99**, 587-594. doi:10.1016/S0049-3848(00)00292-9

- Mithal, D. S., Ren, D. and Miller, R. J. (2013). CXCR4 signaling regulates radial glial morphology and cell fate during embryonic spinal cord development. *Glia* **61**, 1288-1305. doi:10.1002/glia.22515
- Miyazaki, S., Minamida, R., Furuyama, T., Tashiro, F., Yamato, E., Inagaki, S. and Miyazaki, J.-I. (2012). Analysis of Foxo1-regulated genes using Foxo1-deficient pancreatic β cells. *Genes Cells* **17**, 758-767. doi:10.1111/j.1365-2443.2012.01625.x
- Morisada, T., Oike, Y., Yamada, Y., Urano, T., Akao, M., Kubota, Y., Maekawa, H., Kimura, Y., Ohmura, M., Miyamoto, T. et al. (2005). Angiopoietin-1 promotes LYVE-1-positive lymphatic vessel formation. *Blood* **105**, 4649-4656. doi:10.1182/blood-2004-08-3382
- Nagasawa, T., Hirota, S., Tachibana, K., Takakura, N., Nishikawa, S.-I., Kimura, Y., Yoshida, N., Kikutani, H. and Kishimoto, T. (1996). Defects of B-cell lymphopoiesis and bone-marrow myelopoiesis in mice lacking the CXCL chemokine PBSF/SDF-1. *Nature* **382**, 635-638. doi:10.1038/382635a0
- Nakamura, N., Ramaswamy, S., Vazquez, F., Signoretti, S., Loda, M. and Sellers, W. R. (2000). Forkhead transcription factors are critical effectors of cell death and cell cycle arrest downstream of PTEN. *Mol. Cell. Biol.* **20**, 8969-8982. doi:10.1128/MCB.20.23.8969-8982.2000
- Niessen, K., Zhang, G., Ridgway, J. B., Chen, H., Kolumam, G., Siebel, C. W. and Yan, M. (2011). The notch1-Dll4 signaling pathway regulates mouse postnatal lymphatic development. *Blood* **118**, 1989-1997. doi:10.1182/blood-2010-11-319129
- Niessen, K., Zhang, G., Ridgway, J. B., Chen, H. and Yan, M. (2014). ALK1 signaling regulates early postnatal lymphatic vessel development. *Blood* **115**, 1654-1661. doi:10.1182/blood-2009-07-235655
- Niimi, K., Ueda, M., Fukumoto, M., Kohara, M., Sawano, T., Tsuchihashi, R., Shibata, S., Inagaki, S. and Furuyama, T. (2017). Transcription factor FOXO1 promotes cell migration toward exogenous ATP via controlling P2Y1 receptor expression in lymphatic endothelial cells. *Biochem. Biophys. Res. Commun.* **489**, 413-419. doi:10.1016/j.bbrc.2017.05.156
- Norrmén, C., Ivanov, K. I., Cheng, J., Zangger, N., Delorenzi, M., Jaquet, M., Miura, N., Puolakkainen, P., Horsley, V., Hu, J. et al. (2009). FOXC2 controls formation and maturation of lymphatic collecting vessels through cooperation with NFATc1. *J. Cell Biol.* **185**, 439-457. doi:10.1083/jcb.200901104
- Okabe, K., Kobayashi, S., Yamada, T., Kurihara, T., Tai-Nagara, I., Miyamoto, T., Mukoyama, Y.-S., Sato, T. N., Suda, T., Ema, M. et al. (2014). Neurons limit angiogenesis by titrating VEGF in retina. *Cell* **159**, 584-596. doi:10.1016/j.cell.2014.09.025
- Ping, Y.-F., Yao, X.-H., Jiang, J.-Y., Zhao, L.-T., Yu, S.-C., Jiang, T., Lin, M. C. M., Chen, J.-H., Wang, B., Zhang, R. et al. (2011). The chemokine CXCL12 and its receptor CXCR4 promote glioma stem cell-mediated VEGF production and tumour angiogenesis via PI3K/AKT signalling. *J. Pathol.* **224**, 344-354. doi:10.1002/path.2908
- Rinderknecht, M. and Detmar, M. (2008). Tumor lymphangiogenesis and melanoma metastasis. *J. Cell. Physiol.* **216**, 347-354. doi:10.1002/jcp.21494
- Salcedo, R., Wasserman, K., Young, H. A., Grimm, M. C., Howard, O. M. Z., Anver, M. R., Kleinman, H. K., Murphy, W. J. and Oppenheim, J. J. (1999). Vascular endothelial growth factor and basic fibroblast growth factor induce expression of CXCR4 on human endothelial cells: in vivo neovascularization induced by stromal-derived factor-1 α . *Am. J. Pathol.* **154**, 1125-1135. doi:10.1016/S0022-9440(10)65365-5
- Schneider, C. A., Rasband, W. S. and Eliceiri, K. W. (2012). NIH Image to ImageJ: 25 years of image analysis. *Nat. Methods* **9**, 671-675. doi:10.1038/nmeth.2089
- Seoane, J., Le, H.-V., Shen, L., Anderson, S. A. and Massagué, J. (2004). Integration of Smad and forkhead pathways in the control of neuroepithelial and glioblastoma cell proliferation. *Cell* **117**, 211-223. doi:10.1016/S0092-8674(04)00298-3
- Sierro, F., Biben, C., Martínez-Muñoz, L., Mellado, M., Ransohoff, R. M., Li, M., Woehl, B., Leung, H., Groom, J., Batten, M. et al. (2007). Disrupted cardiac development but normal hematopoiesis in mice deficient in the second CXCL12/SDF-1 receptor, CXCR7. *Proc. Natl. Acad. Sci. USA* **104**, 14759-14764. doi:10.1073/pnas.0702229104
- Srinivasan, R. S., Geng, X., Yang, Y., Wang, Y., Mukatira, S., Studer, M., Porto, M. P. R., Lagutin, O. and Oliver, G. (2010). The nuclear hormone receptor Coup-TFII is required for the initiation and early maintenance of Prox1 expression in lymphatic endothelial cells. *Genes Dev.* **24**, 696-707. doi:10.1101/gad.1859310
- Stahl, M., Dijkers, P. F., Kops, G. J. P. L., Lens, S. M. A., Coffey, P. J., Burgering, B. M. T. and Medema, R. H. (2002). The Forkhead Transcription Factor FoxO Regulates Transcription of p27Kip1 and Bim in Response to IL-2. *J. Immunol.* **168**, 5024-5031. doi:10.4049/jimmunol.168.10.5024
- Strasser, G. A., Kaminker, J. S. and Tessier-Lavigne, M. (2010). Microarray analysis of retinal endothelial tip cells identifies CXCR4 as a mediator of tip cell morphology and branching. *Blood* **115**, 5102-5110. doi:10.1182/blood-2009-07-230284
- Takabatake, Y., Sugiyama, T., Kohara, H., Matsusaka, T., Kurihara, H., Koni, P. A., Nagasawa, Y., Hamano, T., Matsui, I., Kawada, N. et al. (2009). The CXCL12 (SDF-1)/CXCR4 axis is essential for the development of renal vasculature. *J. Am. Soc. Nephrol.* **20**, 1714-1723. doi:10.1681/ASN.2008060640
- Tammela, T. and Alitalo, K. (2010). Lymphangiogenesis: molecular mechanisms and future promise. *Cell* **140**, 460-476. doi:10.1016/j.cell.2010.01.045
- Tran, H., Brunet, A., Grenier, J. M., Datta, S. R., Fornace, A. J. J., DiStefano, P. S., Chiang, L. W. and Greenberg, M. E. (2002). DNA repair pathway stimulated by the forkhead transcription factor FOXO3a through the Gadd45 protein. *Science* **296**, 530-534. doi:10.1126/science.1068712
- Wang, Y., Nakayama, M., Pitulescu, M. E., Schmidt, T. S., Bochenek, M. L., Sakakibara, A., Adams, S., Davy, A., Deutsch, U., Lüthi, U. et al. (2010). Ephrin-B2 controls VEGF-induced angiogenesis and lymphangiogenesis. *Nature* **465**, 483-486. doi:10.1038/nature09002
- Wigle, J. T. and Oliver, G. (1999). Prox1 function is required for the development of the murine lymphatic system. *Cell* **98**, 769-778. doi:10.1016/S0092-8674(00)81511-1
- Wilhelm, K., Happel, K., Eelen, G., Schoors, S., Oellerich, M. F., Lim, R., Zimmermann, B., Aspö, I. M., Franco, C. A., Boettger, T. et al. (2016). FOXO1 couples metabolic activity and growth state in the vascular endothelium. *Nature* **529**, 216-220. doi:10.1038/nature16498
- Wuchter, P., Leinweber, C., Saffrich, R., Hanke, M., Eckstein, V., Ho, A. D., Grunze, M. and Rosenhahn, A. (2014). Plerixafor induces the rapid and transient release of stromal cell-derived factor-1 alpha from human mesenchymal stromal cells and influences the migration behavior of human hematopoietic progenitor cells. *Cell Tissue Res.* **355**, 315-326. doi:10.1007/s00441-013-1759-7
- Xu, Y., Yuan, L., Mak, J., Pardanau, L., Caunt, M., Kasman, I., Larrivée, B., Del Toro, R., Suchting, S., Medvinsky, A. et al. (2010). Neuropilin-2 mediates VEGF-C-induced lymphatic sprouting together with VEGFR3. *J. Cell Biol.* **188**, 115-130. doi:10.1083/jcb.200903137
- Yamada, Y., Nezu, J.-I., Shimane, M. and Hirata, Y. (1997). Molecular cloning of a novel vascular endothelial growth factor, VEGF-D. *Genomics* **42**, 483-488. doi:10.1006/geno.1997.4774
- Yokohama-Tamaki, T., Otsu, K., Harada, H., Shibata, S., Obara, N., Irie, K., Taniguchi, A., Nagasawa, T., Aoki, K., Calviari, S. R. et al. (2015). CXCR4/CXCL12 signaling impacts enamel progenitor cell proliferation and motility in the dental stem cell niche. *Cell Tissue Res.* **362**, 633-642. doi:10.1007/s00441-015-2248-y
- Zraggen, S., Huggenberger, R., Kerl, K. and Detmar, M. (2014). An important role of the SDF-1/CXCR4 axis in chronic skin inflammation. *PLoS ONE* **9**, e93665. doi:10.1371/journal.pone.0093665
- Zhuo, W., Jia, L., Song, N., Lu, X. A., Ding, Y., Wang, X., Song, X., Fu, Y. and Luo, Y. (2012). The CXCL12-CXCR4 chemokine pathway: a novel axis regulates lymphangiogenesis. *Clin. Cancer Res.* **18**, 5387-5398. doi:10.1158/1078-0432.CCR-12-0708